Superior catalytic behavior of trace Pt-doped Ni/Mg(Al)O in methane reforming under daily start-up and shut-down operation

Dalin Li,[1] Kazufumi Nishida,[1] Yingying Zhan,[1] Tetsuya Shishido,[2] Yasunori Oumi,[1] Tsuneji Sano[1] and Katsuomi Takehira[1]*

[1]*Department of Chemistry and Chemical Engineering, Graduate School of Engineering, Hiroshima University, Kagamiyama 1-4-1, Higashi-Hiroshima 739-8527, Japan*

[2]*Department of Molecular Engineering, Graduate School of Engineering, Kyoto University, Katsura 1, Nishikyo-ku, Kyoto 615-8510, Japan*

Applied Catalysis A: General, Volume 350, Issue 2, 30 November 2008, Pages 225-236

Received 7 May 2008; Received in revised form 7 August 2008; Accepted 18 August 2008

*Correspondence should be addressed to:

Professor Katsuomi Takehira

Department of Chemistry and Chemical Engineering,

Graduate School of Engineering, Hiroshima University,

Kagamiyama 1-4-1, Higashi-Hiroshima, 739-8527, Japan

Phone : (+81-824)-24-6488

Telefax: (+81-824)-24-6488

E-mail: takehira@hiroshima-u.ac.jp

Abstract

Doping effects of Pt and Ru on Ni/Mg(Al)O catalysts were compared in daily start-up and shut-down operations of steam reforming of CH_4. Trace Pt-doped catalyst showed better behavior than trace Ru-doped catalyst; the former was self-activated but the latter was not, although both exhibited self-regenerative activity. Moreover, the former exhibited sustainable activity, although the latter was quickly passivated, in the autothermal reforming of CH_4. Formation of Pt-Ni alloy on the surface of fine Ni metal particles on the catalysts was suggested by EXAFS analyses. CH_4 was dissociatively activated to form hydrogen on Pt, assisted by adsorbed O or OH species, leading to the self activation via Ni reduction by hydrogen spillover from Pt. The self-regeneration of the Pt-Ni/Mg(Al)O catalysts can be achieved by the continuous rebirth of active Ni metal species via reversible reduction-oxidation between Ni^0 and Ni^{2+} in/on Mg(Ni,Al)O periclase assisted by the hydrogen spillover.

Key Words: CH_4 reforming, self activation, self-regeneration, Ni/Mg(Al)O catalyst, Pt doping, daily start-up and shut-down operation.

1. Introduction

Steam reforming (SR) of hydrocarbons, especially of CH_4, is the most widespread and generally the most economical way to make hydrogen [1]. This process still requires further advancement in the preparation of low cost catalysts with high sustainability. Hydrogen production for polymer electrolyte fuel cells (PEFCs) is a research area of urgent importance in addressing global warming. In contrast to the reformers in large-scale industry processes under stationary operating conditions, the temperature varies frequently due to daily start-up and shut-down (DSS) operations for hydrogen production of PEFCs in domestic use. Between shut-down and start-up in the DSS operation, the catalyst bed in the reformer is purged by steam or air to enhance safety. Thus, a catalyst must be able to tolerate multiple cycles under such unusual transient conditions without deterioration.

We previously reported that Ni/Mg(Al)O catalyst derived from hydrotalcite (HT)-like compounds produced highly dispersed and stable Ni metal particles on the surface [2-4] and were successfully applied in SR and oxidative SR of CH_4 [2,3]. Deactivations of Ni-loaded catalysts were reported to be caused by coking, sintering or oxidation of the active metal species [5,6]. Ni metal can be oxidized not only by gaseous oxygen, but also even in the presence of steam. The Ni/Mg(Al)O catalysts were quickly deactivated due to the oxidation of Ni metal by both oxygen gas and steam when applied in the DSS operation of SR of CH_4 [7].

Recently, we reported that the doping of trace noble metals on the Ni/Mg(Al)O catalysts was effective for suppressing the Ni oxidation during the DSS operation [8,9]. The Ni/Mg(Al)O catalysts doped with traces of noble metals exhibited high and

sustainable activity in the DSS SR of CH_4 [9] and partial oxidation (PO) of propane to synthesis gas [10]. Moreover, we have reported an excellent catalytic behavior, that is, self-regenerative activity of the Ni/Mg(Al)O catalyst doped with trace Ru during the DSS SR of CH_4 [11]. However, the Ru-doped Ni/Mg(Al)O catalyst could not be self-activated in SR of CH_4 and, moreover, was not sustainable enough when it was used in autothermal steam reforming (ATSR) of CH_4, resulting in a drastic deterioration in the catalytic activity. In the present paper, we report both self-activation and self-regenerative activity of trace Pt-doped Mg(Ni,Al)O catalyst. We also report its sustainable activity not only in DSS SR but also in ATSR of CH_4. The effects of Pt doping on such catalytic behavior have been carefully investigated and compared with those of Ru doping [11].

2. Experimental

2.1. Catalyst preparation

Ni-loaded Mg(Al)O catalyst with the Mg/Ni/Al atomic ratio of 2.5/0.5/1 was prepared by co-precipitation as described previously [2-4]; $Mg_{2.5}(Ni_{0.5})$-Al HT-like precursor, in which a part of Mg^{2+} in Mg-Al HT was replaced by Ni^{2+}, was prepared by co-precipitation of the nitrates of metal components. An aqueous solution containing the nitrates of Mg^{2+}, Ni^{2+} and Al^{3+} was added slowly into an aqueous solution of sodium carbonate at room temperature and at pH = 10.0. After the solution was aged at 60 ºC for 12 h, the precipitate was washed with de-ionized water and dried in air at 100 ºC. The $Mg_{2.5}(Ni_{0.5})$-Al HT-like precursor was calcined in a muffle furnace in a static air atmosphere by increasing the temperature from ambient temperature to 850 ºC at a rate

of 0.83 ºC min^{-1} and maintaining it at 900 ºC for 5 h, to form $Mg_{2.5}(Al,Ni_{0.5})O$ periclase as the precursor of $Ni_{0.5}/Mg_{2.5}(Al)O$ catalyst. The periclase materials were obtained as powders, and the Ni loading was found to be 16.0 wt% by inductively coupled plasma spectroscopy analyses after the calcination at 850 ºC.

Pt, Rh or Ru doping was done by adopting a "memory effect" of Mg(Ni)-Al HT [8]; a 1.0 g portion of $Mg_{2.5}(Al,Ni_{0.5})O$ periclase powders was dipped in an aqueous solution of Pt(II), Rh(III) or Ru(III) nitrate for 1 h at room temperature, followed by drying in air at 100 ºC. A prescribed amount of Pt(II), Rh(III) or Ru(III) nitrate was dissolved in 5 ml of de-ionized water. Mg(Ni)-Al HT was reconstituted from $Mg_{2.5}(Ni_{0.5},Al)O$ periclase during the dipping due to a "memory effect." During this reconstitution, both Pt and Ru were physically trapped, whereas Rh(III) was chemically replaced at the Al(III) sites, in the layered structure of the HT [12]. The sample was finally calcined at 850 ºC for 5 h and the precursors of Pt-, Rh- or Ru-doped $Ni_{0.5}/Mg_{2.5}(Al)O$ catalysts were obtained. The precursor powder was pressed to a disc, crushed roughly, and sieved to the particle sizes of 0.36 - 0.60 mm in a diameter and used in the reforming reactions.

As a control, 13.5 wt% Ni/γ-Al_2O_3 catalyst was prepared by the incipient wetness method using γ-Al_2O_3 (JRC-ALO8) and an aqueous solution of Ni(II) nitrate, followed by calcination at 850 ºC for 5 h.

2.2. Characterization of catalyst

The structures of the catalysts were studied by using powder X-ray diffraction (XRD), transmission electron microscopy (TEM), X-ray absorption (XANES and EXAFS), inductively coupled plasma optical emission spectrometry (ICP), temperature

programmed reduction (TPR), temperature programmed oxidation (TPO), and N_2 and H_2 adsorption.

XRD was recorded on a Mac Science MX18XHF-SRA powder diffractometer with mono-chromatized Cu Kα radiation (λ = 0.154 nm) at 40 kV and 30 mA. The diffraction pattern was identified through comparison with those included in the JCPDS (Joint Committee of Powder Diffraction Standards) database. The size of Ni metal particles on the catalyst was calculated from Scherrer's equation: $d = K\lambda/\beta\cos\theta$; β, full width at half maximum; $K = 0.94$ and $\lambda = 1.5405$ Å.

TEM images were obtained on a FE-TEM Hitachi HF-2200 instrument. The samples were crushed to fine powders, dispersed in heptane using supersonic waves, and deposited on a Cu TEM grid with a holey carbon film.

Ni *K*-edge, Ru *K*-edge and Pt L_3-edge XAFS spectra were measured at the BL01B1 station of the SPring-8 with the approval of the Japan Synchrotron Radiation Research Institute (JASRI) (proposal 2006A1217). The storage ring was operated at 8 GeV with a ring current of 98-100 mA. A double mirror system was used to avoid higher harmonics in the X-ray beam. A Si(111) single crystal was used to obtain a monochromatic X-ray beam. Ni *K*-edge XAFS spectra were measured in transmission mode by using two ion chambers filled with N_2 (I_0) and 25% Ar diluted with N_2 (I). Ru *K*-edge XAFS spectra were measured in transmission and fluorescence modes using ion chambers [50% Ar diluted with N_2 (I_0) and 75% Ar diluted with Kr (I)] and a Lytle detector (100% Kr), respectively. Pt L_3-edge XAFS spectra were measured in transmission and fluorescence modes using ion chambers [15% Ar diluted with N_2 (I_0) and 50% Ar diluted with N_2 (I)] and a Lytle detector (100% Kr), respectively. Analyses of EXAFS data were performed using the REX2000 program (Version: 2.5.7; Rigaku

Corp.). For EXAFS analyses, the oscillation was first extracted from EXAFS data using a spline-smoothing method [13]. The oscillation was normalized by an edge height ca. 50 eV higher than the adsorption edge. For the curve-fitting analysis, the empirical phase shift and amplitude functions for the Ni-Ni, Ru-Ru and Pt-Pt bonds were extracted from data for Ni and Pt foils and Ru metal powder, respectively. Theoretical functions for the Ru–Ni, Pt-Ni, Ni-O and Ru-O bonds were calculated using the FEFF8.2 program [14]. The 0.50 wt% Ru- or Pt-doped $Ni_{0.5}/Mg_{2.5}(Al)O$ sample was used for this measurement in order to guarantee the accuracy of the analytical results.

ICP measurements were performed with a Seiko SPS 7700. The content of each metal component was determined after the sample was completely dissolved using diluted hydrochloric acid and a small amount of hydrofluoric acid.

TPR of the catalyst were performed at a heating rate of 10 ºC min^{-1} using a H_2/Ar (5/95 ml min^{-1}) mixed gas as reducing gas after passing through a 13X molecular sieve trap to remove water. A U-shaped quartz tube reactor (6 mm i.d.) equipped with a thermal conductivity detector for monitoring H_2 consumption was used. Before the TPR measurements, the sample was calcined at 300 ºC for 2 h in an O_2/Ar (10/40 ml min^{-1}) mixed gas.

TPO experiments were performed on the catalyst after the steaming at 900 ºC for 10 h, followed by the stationary SR of CH_4 at 700 ºC for 3 h, from room temperature to 900 ºC at a heating rate of 2.5 ºC min^{-1} in an O_2/N_2 (5/20 ml min^{-1}) mixed gas. The amount of coke formed on the catalyst was estimated from the amount of CO_2 formed during the TPO experiment. No CO was detected during TPO.

The N_2 adsorption (-196 ºC) study was conducted to examine the BET surface area of the samples after the calcination. The measurement was carried out on a

Bell-Japan Belsorp-mini. The samples were pretreated in N_2 at 200 ºC for 10 h before the measurements were obtained.

Ni dispersion was determined by static equilibrium adsorption of H_2 at ambient temperature using the pulse method. A 50-mg catalyst sample was reduced at 900 ºC in a H_2/N_2 (5/20 ml min^{-1}) mixed gas for 1 h, and this reduced catalyst was used for the measurement. During the pulse experiment, the amount of H_2 was monitored by a TCD gas chromatograph. Uptake of H_2 at monolayer coverage of the Ni species was used to estimate Ni metal dispersion and particle size. The equation used to calculate dispersion was:

$$\%D = 1.17\,X / Wf \quad (1)$$

where X is H_2 uptake in μmol g^{-1} of catalyst, W is the weight percent of nickel, and f is the fraction of nickel reduced to the metal, assumed to be 80 % for the HT-derived catalysts [9] and 100 % for the impregnated catalyst. The average crystallite diameters, d, were calculated from $\%D$, assuming spherical metal crystallites [15]:

$$d = 971 / (\%D) \quad (2)$$

2.3. Kinetic measurements

SR was conducted in a fixed-bed flow reactor with a $CH_4/H_2O/N_2$ (50/100/25 ml min^{-1}) mixed gas at 700 ºC over 50 mg of the catalyst in a stationary or a DSS-like mode as reported previously [11]. The catalyst was used as particles (0.36 - 0.60 mm in diameter) dispersed in 50 mg of quartz beads. A U-shaped quartz reactor was used, with the catalyst bed near the bottom. N_2 was used as an internal standard for calculating the CH_4 conversion and the product yields. To test the ability of self-activation of the catalyst, we conducted the stationary operation of SR or PO in a $CH_4/H_2O/N_2$

(50/100/25 ml min^{-1}) or a $CH_4/O_2/N_2$ (50/25/25 ml min^{-1}) gas mixture at 700 ºC for 180 min, after heating the catalyst from room temperature to 700 ºC in N_2 (25 ml min^{-1}) gas flow. In the DSS SR, the reaction was started at 700 ºC after the catalyst was pre-reduced in a H_2/N_2 (5/25 ml min^{-1}) mixed gas at 900 ºC for 30 min. After the reaction at 700 ºC, the reactor was cooled to 200 ºC under steam purging with a H_2O/N_2 (100/25 ml min^{-1}) mixed gas. The reactor was maintained at 200 ºC for 30 min, after which the temperature was again increased to 700 ºC still under the purging conditions. When the temperature reached 700 ºC, the reaction was again started by adding CH_4 (50 ml min^{-1}) into the purging gas. The reaction was carried out at 700 ºC, followed by steam purging. Thus the cycle reaction was repeated four times to perform the DSS-like operation. To test the sustainability under an oxidative atmosphere, we applied air purging with an O_2/N_2 (25/25 ml min^{-1}) gas mixture combined with steam purging; such purging conditions are expressed as, e.g., “air - steam - air”, which means the purging by “air (700 ºC → 200 ºC) - steam (at 200 ºC) - air (200 ºC → 700 ºC)”. In the ATSR of methane, a $CH_4/H_2O/O_2/N_2$ (50/100/25/25 ml min^{-1}) mixed gas was used under the steam purging. The thermocouple to control the reaction temperature was placed at the center of the catalyst bed. In each SR or ATSR step at 700 ºC, analyses of product gases by online TCD-gas chromatography were started after the gas-flow of $CH_4/H_2O/N_2$ or $CH_4/H_2O/O_2/N_2$ mixture was stabilized.

Steaming treatment of the catalyst was carried out using the fixed bed flow reactor in a $H_2/H_2O/N_2$ (20/100/25 ml min^{-1}) mixed gas flow for 10 h at 900 ºC. Each 300 mg of the catalyst was steamed, and a 50-mg catalyst sample after steaming was used for the catalytic reaction in both the stationary and DSS operations of SR. The stationary operation was conducted in a $CH_4/H_2O/N_2$ (50/100/25 ml min^{-1}) mixed gas

flow at 700 ºC for 180 min, and the DSS operation was conducted as described above.

Turnover frequency (TOF) was evaluated using the catalysts as powders, because the activity of $Ni_{0.5}/Mg_{2.5}(Al)O$-based catalyst was so high that only a small amount of catalyst was needed to precisely measure the reaction rate in our small reactor. The reaction had to be carried out without channeling in the catalyst bed at low CH_4 conversion and very high space velocity. All catalysts were crushed, and a 10 mg portion of the catalyst powders (0.075 - 0.180 mm in diameter) was dispersed in ca. 20 mg of quartz wool and pretreated in a H_2/N_2 (5/25 ml mi^{-1}) mixed gas flow at 900 ºC for 30 min. The reaction was carried out at either 500 or 600 ºC in a $CH_4/H_2O/N_2$ (88.8/177.6/44.4 ml min^{-1}) mixed gas flow at a GHSV of 1.6×10^6 ml g_{cat}^{-1} h^{-1}. For both FCR and RUA catalysts, the reaction was carried out at a low GHSV of 3.6×10^5 ml g_{cat}^{-1} h^{-1} due to their low activities.

3. Results

3.1. Self-activation of Pt-doped Ni/Mg(Al)O in CH_4 steam reforming.

We briefly reported that 0.1 wt% Rh-, Pt- and Pd-doped $Ni_{0.5}/Mg_{2.5}(Al)O$ catalysts were self-activated during a stationary SR of CH_4 [8]. The effects of the doping amounts of Rh and Ru on the SR were studied in the previous work [16]; Rh was effective for the self-activation with the doping above 0.10 wt%, whereas Ru showed no reforming activity for 3 h even with 0.50 wt% doping without pre-reduction. The effects of the doping amount of Pt on the catalyst self-activation in the stationary SR of CH_4 were studied and the results are shown in Fig. 1 together with those of Rh and Ru. All 0.50, 0.10 and 0.05 wt% Pt-doped $Ni_{0.5}/Mg_{2.5}(Al)O$ exhibited high CH_4

conversion just after starting the reaction, although 0.05 wt% Pt-doping needed a short time of induction period. The ability of noble metals for the self-activation was in the order of Pt > Rh >> Ru; Ru never induced the self-activation even with the 0.50 wt% of doping. This is probably due to the strong ability of Pt followed by Rh to promote CH_4 dissociation to produce hydrogen.

A theoretical study of CH_4 activation, i.e., CH_4 dissociation, was conducted on a number of transition metals M (Ru, Ni, Rh, Ir, Pd, Pt) by simulating the metal M(111) surface by a cluster model [17]. Dehydrogenations of CH_x to CH_{x-1} are highly endothermic in the gas-phase, and the calculated values of dissociation energy, i.e., D, are: CH_3-H, 4.85 eV; CH_2-H, 5.13 eV; CH-H, 4.93 eV; C-H, 3.72 eV [17]. On the metal surface, there is a significant reduction in the D values, owing to the presence of strong metal-CH_{x-1} and metal-H bonds. Summation of the energies for the four discrete steps gives the total dissociation energies, D_{tot}, for $CH_{4,s} \rightarrow C_s + 4H_s$ and should be a more realistic measure for the activity of the metal in CH_4 dissociation. The total dissociation is shown to be quite exothermic on Rh (by -0.7 eV); it is slightly endothermic on Ru (0.01 eV) and Ir (0.3 eV), and it is rather endothermic on Pd and Pt (~1 eV). This indicates that the total dissociation of CH_4 on Rh is thermodynamically the most favorable among the transition metals. The D_{tot} values vary in the order: Rh ≈ Ni < Ru < Ir < Pt < Pd.

On the other hand, in the presence of adsorbed oxygen, oxygen at metal on-top sites promotes CH_4 dehydrogenation; oxygen promotes CH_4 dehydrogenation on Pt, but shows no such effect on the other transition metals [18]. In the presence of adsorbed oxygen, in addition to the direct dissociation of CH_4 on bare metal surfaces, we may consider the following reactions:

$$CH_{x,s} + O_s \rightarrow CH_{x-1,s} + OH_s \quad (x = 4, 3, 2, 1) \qquad (3)$$

Because the H atom binds more strongly with O_s than with the bare metal, the CH_4 dissociation reactions in the presence of chemisorbed oxygen, i.e., O_s, have lower reaction energies due to hydroxyl formation [19,20]. The O_s species increases adsorption energies of H on Pt, but decreases those on the other transition metals. Therefore, O_s promotes CH_4 dissociation on Pt, but does not promote it on the other transition metals.

The results obtained for PO of CH_4 over Ru, Rh- and Pt-doped $Ni_{0.5}/Mg_{2.5}(Al)O$ are depicted in Fig. 2. Pt doping was the most effective for the self-activation of $Ni_{0.5}/Mg_{2.5}(Al)O$; even the material with 0.05 wt % of the doping exhibited a reforming activity and produced hydrogen with high selectivity without induction period. Although 0.01 wt % of Pt doping exhibited CH_4 conversion above 20 %, no H_2 production was observed, while combustion products were detected. The order of noble metals for the self-activation was again Pt > Rh >> R; the effect of "adsorbed oxygen species" has been clearly confirmed. In the present work (Fig. 1), steam was added instead of oxygen, resulting in the formations of plenty of OH_s on the MgO surface, since MgO is thermodynamically unstable compared with $Mg(OH)_2$ under steam atmosphere [21]. MgO reacts even with moisture in the air, especially at low coordination atomic sites, to form $Mg(OH)_2$ brucite; MgO surface was covered by OH_s and further OH_s species migrated from MgO to Pt metal surface and formed Pt-OH species. We may consider that such Pt-OH species can also promote CH_4 dissociation instead of O_s on Pt.

3.2. Activity of Pt-doped Ni/Mg(Al)O in DSS operation.

We previously reported that Ru and Rh doping enhanced the sustainability of $Ni_{0.5}/Mg_{2.5}(Al)O$ during DSS SR of CH_4 [11,16]. Rh metal is expensive, whereas Ru metal is rather cheap. Although oxidized Ru will evaporate and is very hazardous under oxidizing (like ATR conditions) conditions, actually Ru has been frequently used as the reforming catalysts. Unfortunately, the Ru doping was not effective for the self-activation in the stationary SR of CH_4; the Pt doping was the most effective among the noble metals tested (Fig. 1). The effects of doping amount of Pt on $Ni_{0.5}/Mg_{2.5}(Al)O$ in the DSS SR of CH_4 are shown in Fig. 3. The SR always proceeded selectively to H_2, CO and CO_2 following the thermodynamic equilibrium under the condition of S/C = 2/1. Pt-doping with 0.01 wt% showed a total deactivation after the second steam purging due to a very small amount. With Pt doping above 0.03 wt%, the catalysts showed a sustainable activity during the DSS SR, even though the activity, i.e., both CH_4 conversion and rate of H_2 production, decreased just after each steam purging. Such decrease in the activity was more clearly observed with decreasing the Pt doping amount, indicating that Pt assisted the regeneration of the active Ni species.

The physicochemical properties of Pt-doped $Ni_{0.5}/Mg_{2.5}(Al)O$ are shown in Table 1. The specific surface area of $Ni_{0.5}/Mg_{2.5}(Al)O$ decreased by Pt doping. Contrarily, H_2 uptake as well as Ni dispersion increased, while Ni particle size decreased, with increasing the Pt doping, indicating that Ni particles were more finely dispersed by the Pt doping. H_2-TPR measurements of Pt-doped $Ni_{0.5}/Mg_{2.5}(Al)O$ exhibited a clear decrease in Ni reduction temperature from 891 ^oC for $Ni_{0.5}/Mg_{2.5}(Al)O$ (no Pt doping) to 887 ^oC (0.01 wt% Pt), 874 ^oC (0.05 wt% Pt), 850 ^oC (0.10 wt% Pt) and finally to 823 ^oC (0.50 wt% Pt) (Data are not shown). These results indicate that Pt assisted in the reduction of Ni^{2+} in $Mg_{2.5}(Ni_{0.5},Al)O$ periclase [9]. No distinct reduction peak of Pt was

observed, suggesting that all Pt was highly dispersed or existed as Pt-Ni alloy [8]. All these facts may result in an enhancement of the activity as well as the sustainability of Pt-doped $Ni_{0.5}/Mg_{2.5}(Al)O$ catalysts. $Ni_{0.5}/Mg_{2.5}(Al)O$ was completely deactivated due to the Ni oxidation on the catalyst surface [7]. We conclude that Ni was oxidized during the steam purging and further re-reduced by hydrogen spillover from Pt during the SR of CH_4 at 700 ºC as previously reported for the Ru- or Rh-doped Ni/Mg(Al)O catalysts [11,16].

3.3. Effect of steaming on Pt-doped Ni/Mg(Al)O.

The physicochemical properties of supported Ni and Pt-Ni catalysts after steaming in a $H_2/H_2O/N_2$ (20/100/25 ml min^{-1}) mixed gas flow for 10 h at 900 ºC are shown in Table 1. Such steaming treatment causes a severe sintering of supported metal catalysts and is often used to conventionally evaluate the catalyst life. After the steaming, specific surface areas of the $Ni_{0.5}/Mg_{2.5}(Al)O$, 13.5 wt% Ni/γ-Al_2O_3 and 0.10 wt% Pt-$Ni_{0.5}/Mg_{2.5}(Al)O$ catalysts decreased significantly. H_2 uptake also decreased, indicating an increase in Ni particle size. The increase in Ni particle size was also confirmed by the calculations from the line width in the XRD reflections. Ni loading on γ-Al_2O_3 produced highly dispersed Ni particles via a formation of $NiAl_2O_4$ spinel on the catalyst surface [22]. However, on the 13.5 wt% Ni/γ-Al_2O_3, Ni dispersion was lower; Ni particle size was larger compared with those on $Ni_{0.5}/Mg_{2.5}(Al)O$ and all Pt-doped $Ni_{0.5}/Mg_{2.5}(Al)O$ before steaming. In the results obtained by both XRD measurement and H_2 uptake after steaming, Ni sintering was the most significant on the 13.5 wt% Ni/γ-Al_2O_3, followed by the $Ni_{0.5}/Mg_{2.5}(Al)O$ and then by the 0.10 wt% Pt-$Ni_{0.5}/Mg_{2.5}(Al)O$. Pt doping slightly suppressed the sintering of Ni particles.

Although a significant increase in H_2 uptake was observed by 0.10 wt% Pt doping on the $Ni_{0.5}/Mg_{2.5}(Al)O$, the contribution of Pt in H_2 uptake must be negligible, since the chemisorption stoichiometry is H/Pt_s = 1/1 [23] and the molar ratio of Pt/Ni on 0.10 wt% Pt-$Ni_{0.5}/Mg_{2.5}(Al)O$ is calculated as 1/733 for total Ni amount, or at least 1/586 for the surface Ni amount calculated from 80 % of Ni reduction degree [9,24]. Even when we suppose that all Pt species are located on the surface of Ni particles, the direct contribution of Pt on H_2 uptake must be small; some other factors such as surface Pt-Ni alloy formation or decrease in Ni particle size must be considered to explain the increase in H_2 uptake by the Pt doping. We conclude that the Pt doping on the $Ni_{0.5}/Mg_{2.5}(Al)O$ suppressed the sintering of Ni particles during the steaming treatment.

3.4. Activity of Pt-doped Ni/Mg(Al)O after steaming.

DSS SR of CH_4 was carried out between 200 and 700 ºC under steam purging over the catalysts after steaming at 900 ºC (Fig. 4). As previously reported [11,16], both commercial FCR (12 wt%Ni/α-Al_2O_3) and RUA (2 wt%Ru/α-Al_2O_3) were deactivated; FCR was suddenly deactivated just after the first steam purging, whereas RUA was gradually deactivated during the reaction regardless of steam purging. Both $Ni_{0.5}/Mg_{2.5}(Al)O$ and 13.5 wt% Ni/γ-Al_2O_3 showed a complete deactivation just after the first steam purging. Among the catalysts tested, 0.10 wt% Pt-$Ni_{0.5}/Mg_{2.5}(Al)O$ alone showed a stable activity during the DSS SR of CH_4. Judging from the time course of CH_4 conversion during DSS operation (Fig. 4, magnified), one finds interestingly that the activity of 0.10 wt% Pt-$Ni_{0.5}/Mg_{2.5}(Al)O$ was rather stabilized after steaming; a slight decrease in CH_4 conversion observed just after each steam purging disappeared and the CH_4 conversion became almost constant throughout DSS operation after

steaming. A similar phenomenon was also observed for Ru- and Rh-doped Ni/Mg(Al)O [11,16].

Thus, simply Ni supported catalysts were not sustainable for DSS operation, and noble metal doping was effective for the catalyst sustainability. Although 13.5 wt% Ni/γ-Al_2O_3 showed a stable activity in the stationary operation even after steaming, it was not tolerant in DSS operation. The deactivation of the Ni catalysts was due to the Ni oxidation to NiO as seen in the XRD patterns after steaming at 900 ºC followed by DSS SR of CH_4. As previously reported [11,16], a commercial RUA catalyst showed a stable activity in DSS operation, but was deactivated significantly after steaming probably due to the surface passivation of Ru particles by steam. Such deactivation was also observed for 0.1 wt% Ru-$Ni_{0.5}/Mg_{2.5}$(Al)O (vide infra), suggesting that Ru is not as tolerable as Pt and Rh. It must be emphasized that, even after steaming, 0.1 wt% Pt-$Ni_{0.5}/Mg_{2.5}$(Al)O alone showed a high and stable activity not only in stationary operation but also in DSS operation.

3.5. Coking on Pt-doped Ni/Mg(Al)O.

Deactivation of supported Ni catalysts took place by coking, by sintering and by oxidation of active Ni particles. Although remarkable Ni sintering was observed over all $Ni_{0.5}/Mg_{2.5}$(Al)O, 0.10 wt% Pt-$Ni_{0.5}/Mg_{2.5}$(Al)O, and 13.5 wt% Ni/γ-Al_2O_3 after steaming (Table 1), these catalysts showed no severe deactivation. TPO was carried out for the catalysts after steaming followed by stationary SR of CH_4 at 700 ºC. Carbon dioxide alone was produced and no other compound was detected during TPO. The amount of coke materials calculated from the total amount of carbon dioxide produced was as follows: 13.5 wt% Ni/γ-Al_2O_3, 0.11 wt%; $Ni_{0.5}/Mg_{2.5}$(Al)O, 0.70 wt% and 0.10

wt% Pt-$Ni_{0.5}/Mg_{2.5}$(Al)O, 1.12 wt%. As a comparison, 0.10 wt% Ru-$Ni_{0.5}/Mg_{2.5}$(Al)O and 0.10 wt% Rh-$Ni_{0.5}/Mg_{2.5}$(Al)O catalysts showed 0.89 and 0.94 wt % of coking, respectively, after stationary SR of CH_4 [11,16]. Pt was not as effective as Ru and Rh for suppressing coking on $Ni_{0.5}/Mg_{2.5}$(Al)O. This is partly due to a far smaller molar ratio of Pt/Ni (1/532) than those of Rh/Ni (1/281) and Ru/Ni (1/275) for each 0.1 wt % doping. The CO_2 formation during TPO significantly depended on the types of catalyst; both $Ni_{0.5}/Mg_{2.5}$(Al)O and 0.10 wt% Pt-$Ni_{0.5}/Mg_{2.5}$(Al)O showed similar patterns of CO_2 formation; CO_2 began to form at low temperature and several peaks appeared with increasing temperature [11,16]. It has been reported that typical graphite-like coke was ignited at high temperature around 500 ºC, whereas either reactive carbonaceous deposit or chemisorbed CO present on the surface after terminating reaction ignited at temperatures below 400 ºC [25]. Moreover, recent works exhibited that various types of carbon materials including carbon nanofibers can be produced over the Ni catalysts depending on the particle sizes; such products possibly ignited at various temperatures. On both $Ni_{0.5}/Mg_{2.5}$(Al)O and 0.1wt% Pt-$Ni_{0.5}/Mg_{2.5}$(Al)O, CO_2 formation were observed with several peaks between 100 ºC and 400 ºC in the TPO, as reported previously [15]. The amount of coke was the highest on 0.10 wt% Pt-$Ni_{0.5}/Mg_{2.5}$(Al)O, while the deactivation was the lowest,. It is likely that coke materials that formed on 0.10 wt% Pt-$Ni_{0.5}/Mg_{2.5}$(Al)O were not only typical graphitic but also consisted of various types of carbon materials, a part of which can be gasified through the DSS operation.

3.6. TOF of Pt-doped Ni/Mg(Al)O catalysts.

The activities of the catalysts before and after steaming were roughly compared based on the CH_4 conversion (Fig. 4). However, the CH_4 conversions observed over $Ni_{0.5}/Mg_{2.5}(Al)O$-based catalysts were always close to the thermodynamic equilibrium and could not be compared precisely. A more precise evaluation of catalytic activity must be done based on the TOF of the catalyst. TOF of supported Ni catalyst was calculated based on both surface Ni amount and total Ni amount. The results are shown in Table 2 together with those of 0.10 wt% Ru-$Ni_{0.5}/Mg_{2.5}(Al)O$ [11]. TOF values based on total Ni amounts (TOF-t) seem more practically reliable compared with those based on surface Ni amounts (TOF-s), since TOF-s values were severely affected by the sintering of Ni particles. According to the results of TOF-t measurements (Table 2), 13.5 wt% Ni/γ-Al_2O_3 was most severely deactivated, followed by $Ni_{0.5}/Mg_{2.5}(Al)O$ and 0.10 wt% Pt-$Ni_{0.5}/Mg_{2.5}(Al)O$. A decline in TOF value after steaming was more significant on 0.10 wt% Pt-$Ni_{0.5}/Mg_{2.5}(Al)O$ than on 0.10 wt% Ru-$Ni_{0.5}/Mg_{2.5}(Al)O$, probably due to a smaller molar amount of Pt than of Ru. The TOF values of both FCR and RUA were one unit smaller than those of $Ni_{0.5}/Mg_{2.5}(Al)O$-based catalysts; moreover, heavy deactivation occurred on both commercial catalysts after steaming [11,16]. It must be noticed that the TOF value of 0.1 wt% Pt-$Ni_{0.5}/Mg_{2.5}(Al)O$ showed no significant decrease even after steaming treatment.

3.7. XRD patterns of Pt-doped Ni/Mg(Al)O after steaming.

XRD patterns of 0.10 wt% Pt-$Ni_{0.5}/Mg_{2.5}(Al)O$ before and after steaming at 900 ºC, and after further followed by steam purged DSS SR of CH_4, are depicted in Fig. 5. Reflections of Ni metal together with both Mg(Ni,Al)O periclase and $Mg(Ni)Al_2O_4$ spinel were intensified for the catalyst after steaming (Figs. 5b). The Ni particle sizes

calculated by both XRD and H_2 uptake measurements (Table 1) showed heavy Ni sintering after steaming. Moreover, a TEM image of 0.10 wt% Pt-$Ni_{0.5}/Mg_{2.5}$(Al)O showed Ni particle sizes of ca. 40 nm at the maximum (Fig. 6A), also demonstrating heavy sintering after steaming. After steaming, followed by DSS SR of CH_4, Ni metal reflections were weakened and broadened (Fig. 5c), indicating that sintered Ni particles were re-dispersed during DSS SR of CH_4. This was also supported by TEM observation of the catalyst after DSS SR of CH_4 (Fig. 6B).

The 13.5 wt% Ni/γ-Al_2O_3 showed reflection lines of both Ni metal and γ-Al_2O_3 before steaming, whereas Ni metal reflections were intensified and α-Al_2O_3 appeared after steaming. This indicates that Ni particles were sintered (see Table 1) and part of γ-Al_2O_3 was converted to α-Al_2O_3 during steaming. After DSS SR of CH_4, the 13.5 wt% Ni/γ-Al_2O_3 showed NiO reflections, indicating that Ni was oxidized to NiO.

3.8. XANES and EXAFS analyses of Pt-doped Ni/Mg(Al)O.

In the Ni *K*-edge XANES spectra of 0.50 wt% Pt-$Ni_{0.5}/Mg_{2.5}$(Al)O, a preedge at 8,328 eV and a peak at 8,347 eV, along with three peaks at higher energy, were observed after calcination (Fig. 7Aa). The peak shape closely resembled that of mixture of NiO and $NiAl_2O_4$ between 8,335 and 8,345 eV reported by Hungría et al. [26]. Because Ni^{2+} has octahedral coordination in both NiO and Mg(Ni,Al)O periclase, a similar spectrum can be observed for both samples. After reduction (Fig. 7Ab), the edge position became close to that of Ni foil (Fig. 7Af), indicating that the lattice Ni^{2+} in Mg(Al,Ni)O periclase was reduced to metallic Ni. However, the oscillation above the edge is slightly different from that of metal foil, i.e., a shoulder peak at 8,330 eV characteristic of the spectrum for Ni foil was weakened, whilst a sharp peak at 8,347 eV characteristic of the

spectrum for NiO was intensified, compared to the spectrum of Ni foil. These differences suggest that Ni was not fully reduced but existed partly as oxidized state in Mg(Al,Ni)O [11] as reported on silica-coated Ni catalysts [27]. This well coincided with ca. 80-90% of reduction degree for Mg(Al,Ni)O periclase [9,23]. After reduction followed by DSS SR of CH_4 (Fig. 7Ac), the peak at 8,347 eV was intensified, whilst the shoulder at 8,330 eV was weakened, indicating that Ni was oxidized during DSS SR. After steaming at 900 ^oC (Fig. 7Ad), followed by DSS SR of CH_4 (Fig. 7Ae), no significant change appeared in the spectrum, indicating that Ni remained in the metallic state. In the Fourier transforms of k^3-weighted Ni *K*-edge EXAFS spectra, two peaks were observed at 1.66 and 2.56 Å (both non-phase shift corrected) for each sample after calcination (Fig. 7Ba). Hungría et al. [26] reported that two peaks were observed at 1.65 and 2.56 Å (both non-phase shift corrected) for the Fourier transformed EXAFS of NiO and were assigned to Ni-O and Ni-Ni bonding, respectively. After reduction (Fig. 7Bb), both peaks at 1.66 and 2.56 Å disappeared and a new peak appeared at 2.13 Å (non-phase shift corrected), coinciding with that observed for Ni foil as a control (Fig. 7Bf). This bond distance coincided with the value for Ni metal reported by Juan-Juan et al. [27] and indicated that Ni^{2+} in $Mg_{2.5}(Ni_{0.5},Al)O$ periclase was reduced to Ni metal. Pt apparently showed no effect on the spectra of Ni, because the Pt/Ni molar ratio was too small (i.e., 1/106) on 0.5 wt% Pt-$Ni_{0.5}/Mg_{2.5}(Al)O$. After reduction followed by DSS SR of CH_4 (Fig. 7Bc), the peak at 2.13 Å was weakened, whilst both peaks at 1.66 and 2.56 Å were intensified, indicating that Ni was partly oxidized during DSS SR. Both spectra showed no significant change after steaming at 900 ^oC (Fig. 7Bd) and followed by DSS SR of CH_4 (Fig. 7Be), indicating that Ni remained mainly in the metallic state.

In the Pt L_3-edge XANES spectra of 0.50 wt% Pt-$Ni_{0.5}/Mg_{2.5}(Al)O$, an intensified

"white line" peak (electron transition from 2p to 5d) at 11,564 eV, along with some peaks at higher energy, was observed after calcination (Fig. 8Aa). The oscillation and the edge position closely resembled those of PtO_2 (Fig. 8Ag), indicating that Pt was oxidized. Pt foil showed a weak "white line" peak at 11,562 eV and the edge position was lower than that of PtO_2. The absorption intensity of the white line for Pt L_3-edge reflects the vacancy in the 5d orbital of Pt atom and thus is related to the oxidation state [28,29]. The strong white line intensity for the calcined sample (Fig. 8Aa), as well as for PtO_2 (Fig. 8Ag), indicated a high oxidation state for the platinum constituent (Pt^{4+}), whereas for all other samples, i.e., after reduction (Fig. 8Ab), after reduction followed by DSS SR of CH_4 (Fig. 8Ac), after steaming (Fig. 8Ad) and after steaming followed by DSS SR of CH_4 (Fig. 8Ae), the intensity was almost the same as that of Pt foil, indicating that Pt existed mainly in a reduced state. For these samples, the EXAFS region was investigated to obtain information on the nearest neighbor atoms. Fourier-transformed k_3-wighted Pt L_3-edge EXAFS spectra of 0.50 wt% Pt-$Ni_{0.5}$/$Mg_{2.5}$(Al)O during preparation, before and after steaming and further followed by DSS SR of CH_4, are depicted in Fig. 7B as well as those of Pt foil and PtO_2 for comparison. Pt foil exhibited a peak corresponding to Pt-Pt bond with a distance 2.64 Å (non-phase shift corrected) (Fig. 8Bf); PtO_2 showed several peaks, among which a peak due to Pt-O bond appeared at 1.68 Å, whilst another due to Pt-Pt bond appeared at 2.64 Å (both non-phase shift corrected) (Fig. 8Bg) [28,29]. The 0.50 wt% Pt-$Ni_{0.5}$/$Mg_{2.5}$(Al)O exhibited two peaks at 1.68 and 2.98 Å (both non-phase shift corrected) after calcination (Fig. 8Ba); the former is assigned to the Pt-O bond, whereas the latter cannot be assigned to any of the Pt-O, Pt-Pt and Pt-Ni bonds. No peak of Pt-Pt bond suggests that Pt species was highly dispersed on the catalyst surface. The peak that

appeared at 2.25 Å (non-phase shift corrected) after reduction (Fig. 8Bb) can be assigned to the Pt-Ni bond because this value is between 2.13 Å (Ni-Ni bond) and 2.64 Å (Pt-Pt bond) observed for Ni foil and Pt foil, respectively. This peak was observed also after reduction followed by DSS SR of CH_4 (Fig. 8Bc); it weakened and shifted slightly toward a shorter bond length after steaming (Fig. 8Bd), and then it again came back to the original bond length as well as the original shape after steaming followed by DSS SR of CH_4 (Fig. 8Be). This indicates that the Pt-Ni species was stable and survived during DSS SR of CH_4 and moreover regenerated after steaming followed by DSS SR of CH_4.

4. Discussion

4.1. Self-regenerative activity of Pt-doped Ni/Mg(Al)O.

Curve fitting results of Ni *K*-edge EXAFS of 0.50 wt% Pt-$Ni_{0.5}$/$Mg_{2.5}$(Al)O together with Ni foil and NiO are summarized in Table 3. No contribution of Ni-Pt was detected because the molar ratio of Pt/Ni was too small, i.e., 1/106; only Ni-Ni bond was observed around 2.48 Å for all samples. The Ni-O bond appeared at 2.06 Å when the sample was reduced followed by DSS SR of CH_4, indicating that the surface of Ni particles was oxidized during DSS SR. Both coordination number and bond length slightly decreased after steaming, whereas both values were recovered to the original values after steaming followed by DSS SR.

Table 4 shows curve fitting results of Pt L_3-edge EXAFS of 0.50 wt% Pt-$Ni_{0.5}$/$Mg_{2.5}$(Al)O as well as those of Pt foil and PtO_2. Neither Pt-Pt bond nor Pt-O bond was observed but the Pt-Ni bond alone appeared for all samples. The Pt-Ni bond

length was 2.53 Å, which is 0.04 Å longer than the Ni-Ni bond in metallic Ni (2.49 Å) and 0.24 Å shorter than the Pt-Pt bond in metallic Pt (2.77 Å). The coordination number of Pt-Ni shell was 6.8, far smaller than that of Pt foil (12), suggesting that Pt is located in the surface layer of Ni particles. In the present work, Pt was doped on Mg(Al,Ni)O periclase particles by adopting "memory effect" and, therefore, Pt is reasonably located on the surface of Ni particles after calcination, followed by reduction. A similar location was previously observed for Ru-Ni [11] and Rh-Ni [15] systems. The coordination number of the Pt-Ni shell (6.8) was larger than those observed for Ru-Ni (3.5) and Rh-Ni (5.0), indicating that Pt was more deeply incorporated into Ni particles than Ru and Rh on 0.50 wt% Ru- and Rh-$Ni_{0.5}/Mg_{2.5}$(Al)O [11,16]. Moreover, a small increase in coordination number (7.7) after steaming followed by DSS SR of CH_4 indicates that Pt was even more deeply incorporated during such treatment. We conclude that Pt was always located mainly in the surface layer of Ni particles during the reaction.

Chen et al. [30] reported that the surfaces of Pt-Ni bimetallic catalysts prepared by sequential impregnations of Pt and Ni on γ-Al_2O_3 were always Pt-terminated with the Pt/Ni ratio of 1/1, regardless of the sequential order, i.e., first with Pt and then with Ni, or vice versa. This is due to the segregation of Pt to the surface during the hydrogen reduction, as predicted by means of density functional theory (DFT) modeling and, moreover, verified experimentally using Auger electron spectroscopy and high-resolution electron energy loss spectroscopy on single crystal Ni/Pt(111) surfaces [31]. Contrarily, Tomishige et al. [32] reported that sequential impregnation i.e., first Ni followed by Pt, exhibited better catalytic performances than co-impregnation methods in oxidative steam reforming of CH_4. In the present work, Pt-Ni/Mg(Al)O catalysts were prepared by Pt impregnation on Mg(Ni,Al)O periclase, suggesting that Ni particles

were originally enriched with Pt in the surface layer. In fact, no significant change was observed in either the Fourier transforms (Fig. 8Bb-e) or the curve fitting results (Table 4) of Pt L_3-edge EXAFS of 0.50 wt% Pt-$Ni_{0.5}$/$Mg_{2.5}$(Al)O during the reaction, i.e., reduced, reduced-steamed, reduced-DSS and reduced-steamed-DSS. Only the sample after reduction followed by steaming exhibited a small shift and a shape alteration in Pt-Ni peak (Fig. 8Bd) and a greater *Rf* value compared with the other samples (Table 4), suggesting that the Pt-Ni bimetallic structure was somewhat distorted due to heavy Ni sintering after steaming. One should notice that the original Pt-Ni bimetallic structure was recovered by DSS SR of CH_4 even after such heavy sintering (Fig. 8Be and Table 4).

TPR curves of 0.10 wt% Pt-$Ni_{0.5}$/$Mg_{2.5}$(Al)O after reduction exhibited a single peak of the $Ni^{2+} \rightarrow Ni^0$ reduction at 850 ºC (Fig. 9a). After steaming at 900 ºC, the reduction peak was usually separated into two peaks, one at 918 ºC and another at 267 ºC (Fig. 9b). It seems that Ni/Mg(Al)O or Mg(Al,Ni)O periclase was reductively decomposed to large-sized Ni particles and Mg(Al,Ni)O of lower Ni content after steaming. Part of the Ni^{2+} ions in $Mg_{2.5}$($Ni_{0.5}$,Al)O periclase were first reduced to Ni metal, exposed to steaming and finally grew to isolated large-sized Ni particles. Simultaneously Mg(Al,Ni)O periclase lost a part of Ni^{2+}, was exposed to steaming and finally formed the sintered structure containing hard-to-reduce Ni^{2+}. The peak at 267 ºC can be assigned to the isolated Ni particles, whereas the peak at 918 ºC to the hard-to-reduce Ni^{2+}. At low temperature, some other peaks also appeared at 121 and 200 ºC after steaming, indicating a phase separation of Ni-Pt alloy; Pt exhibited reduction peaks at 100-200 °C, whereas Ni was reduced at 250-400 °C in the TPR of supported Pt-Ni bimetallic catalysts [33]. When 0.10 wt% Pt-$Ni_{0.5}$/$Mg_{2.5}$(Al)O after

steaming was exposed to DSS SR of CH_4, the peak at 200 ºC disappeared and the peak at 267 ºC shifted to a higher temperature of 290 ºC, whereas the peak at 918 ºC completely shifted toward a lower temperature of 830 ºC (Fig. 9c). These results suggest that the separated species, i.e., Pt and Ni, were again combined and reconstituted to the original bimetallic phase on the catalyst; Ni metal particles were covered by Ni-Pt alloy on the surface as well as Ni^{2+} in the Mg(Al)O periclase phase.

In the TEM images of 0.10 wt% Pt-$Ni_{0.5}$/$Mg_{2.5}$(Al)O (Fig. 6); the large-sized Ni particles (~40 nm) observed after steaming (Fig. 6A) disappeared and were replaced by small-sized particles (< 20 nm) after followed further by DSS SR of CH_4 (Fig. 6B). This indicates that the sintered Ni particles were redispersed during DSS SR. The TPR results given above, along with the XRD (Fig. 5c) and TEM (Fig. 6) observations of 0.10 wt% Pt-$Ni_{0.5}$/$Mg_{2.5}$(Al)O after steaming followed by DSS SR of CH_4, are important for understanding the catalytic mechanism. Even after severe passivation by steaming at 900 °C, the sintered Ni metal particles were redispersed, and the original active sites were regenerated during DSS SR in the presence of Pt. The sintered Ni particles must be oxidized to Ni^{2+} by steam and are possibly incorporated into Mg(Al,Ni)O periclase. In turn, Ni^{2+} in Mg(Al,Ni)O periclase can be quickly reduced, assisted by hydrogen spillover on Pt metal or Pt-Ni alloy. Such reduction-oxidation between Ni^0 and Ni^{2+} on/in Mg(Ni,Al)O periclase aided by hydrogen spillover on Pt metal or Pt-Ni alloy effectively contributed to the regeneration of activity on the Pt-doped Ni/Mg(Al)O catalysts during DSS SR operation.

4.2. Prominent behaviors of Pt-doped Ni/Mg(Al)O.

Among Rh, Ru and Pt, Ru is frequently used as a reforming catalyst for PEFCs due to the low cost [33]. Although Pt is cheaper than Rh, Pt has been used as oxidation or combustion catalyst but has not been frequently used as a reforming catalyst [36]. Pt possesses a potential of C-H activation (vide supra) [18]. It has been confirmed that Pt doping enhances the activity and, moreover, assists the self-regeneration of active Ni sites on Ni/Mg(Al)O catalyst through CH_4 activation followed by hydrogen spillover.

When we consider down stream of H_2-production for PEFCs, water-gas shift and then CO elimination steps follow SR of CH_4 [1]. It was reported that steam condensation heavily sintered and deactivated Cu-catalysts for CO shift reaction [37,38]. Therefore, purging conditions must be selected to avoid steam condensation. In the present work, steam was replaced totally or partially with air, and the activity of Pt-$Ni_{0.5}/Mg_{2.5}$(Al)O was compared with that of Ru-$Ni_{0.5}/Mg_{2.5}$(Al)O in DSS SR of CH_4. The results are depicted in Fig. 10. Under totally air purging conditions, both catalysts showed high and stable activity in DSS SR of CH_4 between 700 °C and 200 °C (Fig. 10A). Moreover, both CH_4 conversion and H_2 production rate exhibited no detectable decrease just after each air purging. This is in contrast to the previous observation, i.e., CH_4 conversion decreased after every steam purging due to Ni oxidation (Fig. 3) [11]. This indicates that air, or oxygen, as purging gas did not oxidize Ni on either catalyst as steam during DSS operation. However, the combination of air and steam as purging gas quickly deactivated 0.10 wt% Ru-$Ni_{0.5}/Mg_{2.5}$(Al)O; both combined purging of air-steam-air and steam-air-steam totally deactivated the catalyst after the first purging (Fig. 10B). On the contrary, 0.10 wt% Pt-$Ni_{0.5}/Mg_{2.5}$(Al)O was not deactivated by such combined purging (Fig. 10B). Just after each purging, both CH_4 conversion and H_2 production rate decreased, but the values gradually increased and the original values

were recovered during stationary SR of CH_4. This suggests that the regenerative activity works on the Pt-Ni catalyst even under air-steam combined purging. It is concluded that Pt-doped Ni/Mg(Al)O is more sustainable than Ru-doped Ni/Mg(Al)O catalyst under air-steam combined purging.

ATSR seems to be a hopeful candidate for the future PEFCs reformers because the exothermic oxidation can supply the heat for endothermic steam reforming [39]. ATSR of CH_4 was carried out on both Pt- and Ru-$Ni_{0.5}/Mg_{2.5}$(Al)O catalysts in DSS mode under steam purging (Fig. 11). When 0.10 wt% Ru-$Ni_{0.5}/Mg_{2.5}$(Al)O was prepared by calcination under either N_2 or air atmosphere after Ru-doping, the amount of Ru that obtained was 0.095 and 0.077 wt%, respectively, as seen by ICP analyses. This indicates that a small amount of Ru sublimated out as RuO_4 during calcination in air atmosphere. Regardless of such differences in Ru doping, both 0.10 wt% Ru-$Ni_{0.5}/Mg_{2.5}$(Al)O calcined in air and in N_2 exhibited significant deactivation just after the first steam purging, indicating that 0.10 wt% Ru-doping was not sustainable enough in the steam purged DSS ATSR of CH_4. Even when Ru doping was increased up to 0.50 wt%, the activity decreased significantly after the first steam purging. This indicates that Ru was not suitable for DSS ATSR (Fig. 11). Contrarily, 0.10 wt% Pt doping was sustainable enough for the steam purged DSS ATSR of CH_4. We conclude that Pt-doped Ni/Mg(Al)O is more sustainable than Ru-doped Ni/Mg(Al)O not only in air-steam purged DSS SR of CH_4 but also in steam purged DSS ATSR of CH_4.

The Ru *K*-edge XANES spectra of 0.50 wt% Ru-$Ni_{0.5}/Mg_{2.5}$(Al)O after reduction, and after reduction followed by DSS ATSR of CH_4, are depicted in Fig. 12A. Ru metal as a control showed a peak at 22,124 eV, along with a preedge at 22,105 eV and some characteristic peaks at the higher energy (Fig. 12Aa). These values are slightly lower

than those reported by Hosokawa et al. [40] (i.e., a preedge at 22,115 eV and a peak at 22,128 eV). After reduction, 0.50 wt% Ru-$Ni_{0.5}/Mg_{2.5}$(Al)O showed a peak at 22,124 eV, along with a pre-edge at 22,105 eV and a shoulder at 22,136 eV (Fig. 12Ab), and some characteristic peaks at the higher energy. These results suggest that Ru was mainly reduced to metallic state, but was partly oxidized, judging from the shoulder at 22,136 eV [41]. It was reported that bulk RuO_2 on Ru/CeO_2 showed a main peak between 22,130 and 22,148 eV [42]. After reduction followed by DSS ATSR of CH_4, the pre-edge at ca. 22,105 eV disappeared and, moreover, the peak at 22,124 eV and especially the shoulder at 22,136 eV were intensified, indicating that Ru was considerably oxidized [40,42].

Such Ru oxidation after DSS ATSR of CH_4 was also supported by the Fourier transforms of k^3-weighted Ru *K*-edge EXAFS spectra of 0.50 wt% Ru-$Ni_{0.5}/Mg_{2.5}$(Al)O (Fig. 12B). Ru metal as a reference exhibited an intensive peak at 2.27 Å (non-phase shift corrected), corresponding to the Ru-Ru bond in metallic Ru (Fig. 12Ba) [41]. After reduction, 0.50 wt% Ru-$Ni_{0.5}/Mg_{2.5}$(Al)O showed a peak at a little shorter distance, i.e., 2.08 Å (non-phase shift corrected), tentatively assigned to the Ru-Ni bond due to the formation of Ni-Ru alloy (Fig. 12Bb). After reduction followed by DSS ATSR of CH_4, the peak shifted toward further shorter distance, i.e., 1.58 Å (non-phase shift corrected), due to the formation of Ru-O bond [41] by Ru oxidation. We previously reported that part of Ru was separated as RuO_2 from the Ru-Ni binary system when Ru-doped Ni/Mg(Al)O catalyst was passivated by steaming at 900 ^oC [11]. Hosokawa et al. [42] observed a peak at 3.0 Å (non-phase shift corrected) for bulk RuO_2 supported on CeO_2 and assigned it to Ru-Ru bonding in the bulk RuO_2. In the present work, no such peak

was observed (Fig. 12Bc), suggesting that RuO_2 was dispersed and isolated on 0.50 wt% Ru-$Ni_{0.5}$/$Mg_{2.5}$(Al)O passivated by DSS ATSR.

Table 5 shows curve fitting results of Ru *K*-edge EXAFS of 0.50 wt% Ru-$Ni_{0.5}$/$Mg_{2.5}$(Al)O. Neither Ru-Ru nor Ru-O bonds were observed but Ru-Ni bonds alone appeared for the catalyst after reduction. The Ru-Ni bond length was 2.49 Å, very close to the Ni-Ni bond in metallic Ni (2.49 Å) and 0.17 Å shorter than the Ru-Ru bond in metallic Ru (2.66 Å). The coordination number of Ru-Ni shell was 3.7, far smaller than that of the Ru metal (12), suggesting that Ru is located in the surface layer of Ni particles, as reported in the previous paper [11]. After reduction followed by DSS ATSR of CH_4, the Ru-Ni shell disappeared and Ru-O shell was found at 2.07 Å, indicating that Ru was separated as RuO_2 from the Ru-Ni binary system. Such phase separation is reasonably accompanied by the corruption of the active sites, resulting in the catalyst deactivation due to the Ni oxidation (Fig. 11).

It must be emphasized that trace Pt-doped Ni/Mg(Al)O exhibited sustainable activity under oxidative conditions, i.e., steam-oxygen mixed purging and ATSR. Moreover this catalyst was self-activated and exhibited self-regenerative activity as well as high TOF values in DSS SR of CH_4. The self-activation was performed by hydrogen-spillover from Pt and, moreover, the self-regeneration was achieved by the continuous rebirth of active Ni species (Scheme 1), that is assisted by both $Ni^{2+} \rightarrow Ni^0$ reduction by the hydrogen spillover and by reversible reduction-oxidation between Ni^0 and Ni^{2+} in/on Mg(Ni,Al)O periclase.

5. Conclusion

Ni/Mg(Al)O catalyst doped with trace Pt was self-activated and, moreover, exhibited self-regenerative activity during DSS SR of CH_4. Although Ru-Ni/Mg(Al)O was quickly deactivated, Pt-Ni/Mg(Al)O exhibited sustainable activity under oxidative conditions. CH_4 was dissociatively activated to form hydrogen on Pt; leading to the self activation via Ni reduction by hydrogen spillover from Pt. Pt-Ni alloy was formed on the surface of fine Ni particles on the catalysts. The Pt-Ni/Mg(Al)O catalyst was passivated by oxidative incorporation of Ni^0 to Ni^{2+} in Mg(Ni,Al)O periclase, whereas trace Pt assisted the regeneration of Ni metal from the Ni^{2+} by hydrogen spillover. The self-regeneration of Pt-Ni/Mg(Al)O can be achieved by the continuous rebirth of active Ni species via reversible reduction-oxidation between Ni^0 and Ni^{2+} in/on Mg(Ni,Al)O periclase assisted by hydrogen spillover from Pt.

References

[1] J.R. Rostrup-Nielsen, Catal. Today 71 (2002) 243-247.

[2] K. Takehira, T. Shishido, P. Wang, T. Kosaka, K. Takaki, Phys. Chem. Chem. Phys. 5 (2003) 3801-3810.

[3] K. Takehira, T. Shishido, P. Wang, T. Kosaka, K. Takaki, J. Catal. 221 (2004) 43-54.

[4] K. Takehira, T. Kawabata, T. Shishido, K. Murakami, T. Ohi, D. Shoro, M. Honda, K. Takaki, J. Catal. 231 (2005) 92-104.

[5] V.A. Tsipouriari, Z. Zhang, X.E. Verukios, J. Catal. 179 (1998) 283-291.

[6] H.S. Bengaard, J.K. Nørskov, J. Sehested, B.S. Clausen, L.P. Nielsen, A.M. Molenbroek, J.R. Rostrup-Nielsen, J. Catal. 209 (2002) 365-384.

[7] T. Ohi, T. Miyata, D. Li, T. Shishido, T. Kawabata, T. Sano, K. Takehira, Appl. Catal. A 308 (2006) 194-203.

[8] T. Miyata, D. Li, M. Shiraga, T. Shishido, Y. Oumi, T. Sano, K. Takehira, Appl. Catal. A 310 (2006) 97-104.

[9] T. Miyata, M. Shiraga, D. Li, I. Atake, T. Shishido, Y. Oumi, T. Sano, K. Takehira, Catal. Commun. 8 (2007) 447-451.

[10] M. Shiraga, D. Li, I. Atake, T. Shishido, Y. Oumi, T. Sano, K. Takehira, Appl. Catal. A 318 (2007) 143-154.

[11] D. Li, I. Atake, T. Shishido, Y. Oumi, T. Sano, K. Takehira, J. Catal. 250 (2007) 299-312.

[12] F. Basile, G. Fornasari, E. Pluzzi, A. Vaccari, Appl. Clay Sci. 13 (1998) 329-345.

[13] J. W. Cook, D.E. Sayers, J. Appl. Phys. 52 (1981) 5024-5031.

[14] A.L. Ankudinov, B. Ravel, J.J. Rehr, S.D. Conradson, Phys. Rev. B 58 (1998) 7565-7576.

[15] C.H. Bartholomew, R.B. Pannell, J.L. Butler, J. Catal. 65 (1980) 335-347.

[16] D. Li, T. Shishido, Y. Oumi, T. Sano, K. Takehira, Appl. Catal. A 332 (2007) 98-109.

[17] M.-S. Liao, Q.-E Zhang, J. Mol. Catal. A 136 (1998) 185-194.

[18] C.-T. Au, C.-F. Ng, M.-S. Liao, J. Catal. 185 (1999) 12-22.

[19] C.-T. Au, H.-Y. Wang, J. Catal. 167 (1997) 337-345.

[20] C.-T. Au, M.-S. Liao, C.-F. Ng, J. Phys. Chem. A 102 (1998) 3959-3969.

[21] J.H. Eun, J.H. Lee, S.G. Kim, M.Y. Um, S.Y. Park, H.J. Kim, Thin Solid Films 435 (2003) 199-204.

[22] N. Sahli, C. Petit, A.C. Roger, A. Kienneman, S. Libs, M.M. Bettebar, Catal. Today 113 (2006) 187-193.

[23] L. Hu, K.A. Boateng, J. M. Hill, J. Mol. Catal. A 259 (2006) 51-60.

[24] A. Olafsen, Å. Slagtern, I.M. Dahl, U. Olsbye, Y. Schuurman, C. Mirodatos, J. Catal. 229 (2005) 163-175.

[25] M.C.J. Bradford, M.A. Vannice, Appl. Catal. A 142 (1996) 73-96.

[26] A.B. Hungría, N.D. Browning, R.P. Erni, M. Fernández-García, J.C. Conesa, J.A. Pérez-Omil, A. Martínez-Arias, J. Catal. 235 (2005) 251-261.

[27] J. Juan-Juan, M.C. Román-Martínez, M.J. Illán-Gómez, Appl. Catal. A 301 (2006) 9-15.

[28] S. Hamada, K. Ikeue, M. Machida, Appl. Catal. B 71 (2007) 1-6.

[29] M. Casapu, J.-D. Grunwaldt, M. Maciejewski, A. Baiker, S. Eckhoff, U. Göbel, M. Wittrock, J. Catal. 251 (2007) 28-38.

[30] Y. Shu, L.E. Murillo, J.P. Bosco, W. Hang, A.I. Frenkel, J.G. Chen, Appl. Catal. A 339 (2008) 169-179.

[31] C.A. Menning, H.H. Hwu, J.G. Chen, J. Phys. Chem. B 110 (2006) 15471-15477.

[32] B. Li, S. Kado, Y. Mukainakano, T. Miyazawa, T. Miyao, S. Naito, K. Okumura, K. Kunimori, K. Tomishige, J. Catal. 245 (2007) 144-155.

[33] B. Pawelec, S. Damynova, K. Arishtirova, J.L.G. Fierro, L. Petrov, Appl. Catal. A 323 (2007) 188-201.

[34] T. Suzuki, H. Iwanami, T. Yoshinari, Int. J. Hydrogen Energy 25 (2000) 119-126.

[35] J. Zheng, J.J. Strohm, C. Song, Fuel Process. Technol. 89 (2008) 440-448.

[36] T.F. Garetto, E. Rincón, C.R. Apesteguía, Appl. Catal. B 73 (2007) 65-72.

[37] O. Ilinich, W. Ruettinger, X.-S Liu, R. Farrauto, J. Catal. 247 (2007) 112-118.

[38] K. Nishida, I. Atake, D. Li, T. Shishido, Y. Oumi, T. Sano, K. Takehira, Appl. Catal. A 337 (2008) 48-57.

[39] B.J. Dreyer, I.C. Lee, J.J. Krummenacher, L.D. Schmidt, Appl. Catal. A 307 (2006) 184-194.

[40] S. Hosokawa, S. Nogawa, M. Taniguchi, K. Utani, H. Kanai, S. Imamura, Appl. Catal. A 288 (2005) 67-73.

[41] C. Roth, N. Benker, M. Mazurek, F. Scheiba, H. Fuess, Appl. Catal. A 319 (2007) 81-90.

[42] S. Hosokawa, M. Taniguchi, K. Utani, H. Kanai, S. Imamura, Appl. Catal. A 289 (2005) 115-120.

Figure captions

Fig. 1 Self-activation of Pt-, Rh- and Ru-$Ni_{0.5}/Mg_{2.5}(Al)O$ with various doping amounts in stationary SR of CH_4.

●, 0.50 wt% Pt-$Ni_{0.5}/Mg_{2.5}(Al)O$; ■, 0.10 wt% Pt-$Ni_{0.5}/Mg_{2.5}(Al)O$; ▲, 0.05 wt% Pt-$Ni_{0.5}/Mg_{2.5}(Al)O$; ♦, 0.01 wt% Pt-$Ni_{0.5}/Mg_{2.5}(Al)O$; ○, 0.50 wt% Rh-$Ni_{0.5}/Mg_{2.5}(Al)O$; □, 0.10 wt% Rh-$Ni_{0.5}/Mg_{2.5}(Al)O$; Δ, 0.05 wt% Rh-$Ni_{0.5}/Mg_{2.5}(Al)O$; ×, 0.50 wt% Ru-$Ni_{0.5}/Mg_{2.5}(Al)O$; +, 0.10 wt% Ru-$Ni_{0.5}/Mg_{2.5}(Al)O$.

Fig. 2 Self-activation of Pt-, Rh- and Ru-$Ni_{0.5}/Mg_{2.5}(Al)O$ with various doping amounts in stationary PO of CH_4.

●, 0.50 wt% Pt-$Ni_{0.5}/Mg_{2.5}(Al)O$; ■, 0.10 wt% Pt-$Ni_{0.5}/Mg_{2.5}(Al)O$; ▲, 0.05 wt% Pt-$Ni_{0.5}/Mg_{2.5}(Al)O$; ♦, 0.01 wt% Pt-$Ni_{0.5}/Mg_{2.5}(Al)O$; ○, 0.50 wt% Rh-$Ni_{0.5}/Mg_{2.5}(Al)O$; □, 0.10 wt% Rh-$Ni_{0.5}/Mg_{2.5}(Al)O$; ×, 0.50 wt% Ru-$Ni_{0.5}/Mg_{2.5}(Al)O$; +, 0.10 wt% Ru-$Ni_{0.5}/Mg_{2.5}(Al)O$.

Fig. 3 DSS SR of CH_4 over Pt-$Ni_{0.5}/Mg_{2.5}(Al)O$ with various Pt doping percentages under steam purging.

Full line, CH_4 conversion; dotted line, rate of H_2 production.

○, 0.01 wt% Pt-$Ni_{0.5}/Mg_{2.5}(Al)O$; □, 0.03 wt% Pt-$Ni_{0.5}/Mg_{2.5}(Al)O$; ■, 0.05 wt% Pt-$Ni_{0.5}/Mg_{2.5}(Al)O$; ●, 0.10 wt% Pt-$Ni_{0.5}/Mg_{2.5}(Al)O$; ▲, 0.50 wt% Pt-$Ni_{0.5}/Mg_{2.5}(Al)O$.

Fig. 4 Comparison of the activity of supported Ni catalysts before and after steaming at 900 ^{o}C for 10 h in steam purged DSS SR of CH_4.

Full line, before steaming; dotted line, after steaming.

Reaction conditions: $CH_4/H_2O/N_2$ = 50/100/25 ml min^{-1}; 700 ºC; catalyst, 50 mg.

●, 0.10 wt% Pt-$Ni_{0.5}/Mg_{2.5}$(Al)O; ○, $Ni_{0.5}/Mg_{2.5}$(Al)O; ▲, 13.5 wt% Ni/γ-Al_2O_3.

Fig. 5 XRD patterns of 0.1 wt% Pt-$Ni_{0.5}/Mg_{2.5}$(Al)O after reduction, after steaming at 900 ºC and after further followed by steam purged DSS SR of CH_4.

a) 0.10 wt% Pt-$Ni_{0.5}/Mg_{2.5}$(Al)O after reduction; b) 0.10 wt% Pt-$Ni_{0.5}/Mg_{2.5}$(Al)O after steaming at 900 ºC; c) 0.10 wt% Pt-$Ni_{0.5}/Mg_{2.5}$(Al)O after steaming at 900 ºC followed by the DSS SR.

●, Ni metal; ○, Mg(Ni,Al)O periclase; □, $MgAl_2O_4$ spinel.

Fig. 6 TEM images of 0.10 wt% Pt-$Ni_{0.5}/Mg_{2.5}$(Al)O after steaming (A) and after further followed by DSS SR of CH_4 (B).

Fig. 7 Ni *K*-edge XANES (A) and Fourier transforms of k^3-weighted Ni *K*-edge EXAFS (B) spectra of 0.50 wt% Pt-$Ni_{0.5}/Mg_{2.5}$(Al)O during preparation, before and after steaming and further followed by DSS SR of CH_4.

a) after calcination; b) after reduction; c) after reduction followed by DSS SR; d) after steaming at 900 ºC; e) after steaming followed by DSS SR; f) Ni foil.

Fig. 8 Pt L_3-edge XANES (A) and Fourier transforms of k^3-weighted Pt L_3-edge EXAFS (B) of 0.50 wt% Pt-$Ni_{0.5}/Mg_{2.5}$(Al)O during preparation, before and after steaming and further followed by DSS SR of CH_4.

A'; A at higher magnification.

a) after calcination; b) after reduction; c) after reduction followed by DSS SR; d) after steaming at 900 ºC; e) after steaming followed by DSS SR; f) Pt foil; g) PtO_2.

Fig. 9 TPR profiles of 0.10 wt% Pt-$Ni_{0.5}/Mg_{2.5}$(Al)O before and after steaming at 900 ^{o}C followed by DSS SR of CH_4.

a) after reduction; b) after steaming at 900 ^{o}C; c) after steaming at 900 ^{o}C followed by DSS SR.

Fig. 10 Comparison of the activities of Pt-$Ni_{0.5}/Mg_{2.5}$(Al)O and Ru-$Ni_{0.5}/Mg_{2.5}$(Al)O in DSS SR of CH_4 under various purging conditions.

Full line, CH_4 conversion; dotted line, rate of H_2 production.

A, ●, 0.10 wt% Pt-$Ni_{0.5}/Mg_{2.5}$(Al)O under air purging; ■, 0.10 wt% Ru-$Ni_{0.5}/Mg_{2.5}$(Al)O under air purging.

B, ●, 0.10 wt% Pt-$Ni_{0.5}/Mg_{2.5}$(Al)O under air-steam-air purging; ■, 0.10 wt% Ru-$Ni_{0.5}/Mg_{2.5}$(Al)O under air-steam-air purging; ○, 0.10 wt% Pt-$Ni_{0.5}/Mg_{2.5}$(Al)O under steam-air-steam purging; □0.10 wt% Ru-$Ni_{0.5}/Mg_{2.5}$(Al)O under steam-air-steam purging;

Fig. 11 Comparison of the activities of Pt-$Ni_{0.5}/Mg_{2.5}$(Al)O and Ru-$Ni_{0.5}/Mg_{2.5}$(Al)O in DSS ASTR of CH_4.

Full line, CH_4 conversion; dotted line, rate of H_2 production.

●, 0.10 wt% Pt-$Ni_{0.5}/Mg_{2.5}$(Al)O; ○, 0.50 wt% Ru-$Ni_{0.5}/Mg_{2.5}$(Al)O; ■, 0.10 wt% Ru-$Ni_{0.5}/Mg_{2.5}$(Al)O calcined in air; ▲, 0.10 wt% Ru-$Ni_{0.5}/Mg_{2.5}$(Al)O calcined in N_2.

Fig. 12 Ru *K*-edge XANES (A) and Fourier transforms of k^3-weighted Ru *K*-edge EXAFS (B) spectra of 0.50 wt% R-$Ni_{0.5}/Mg_{2.5}$(Al)O before and after DSS ASTR of CH_4.

a) Ru foil; b) 0.50 wt% Ru-$Ni_{0.5}/Mg_{2.5}$(Al)O after reduction; c) 0.50 wt% Ru-$Ni_{0.5}/Mg_{2.5}$(Al)O after DSS ASTR.

Scheme 1. The self-activation and self-regenerative activity of trace Pt-doped Ni/Mg(Al)O catalyst.

Table 1. Physicochemical properties of supported metal catalysts before and after steaming.[a]

Catalyst	Specific surface area[b] (m^2 g_{cat}^{-1})		H_2 uptake[c] (μmol g_{cat}^{-1})		Dispersion[d] (%)		Ni (Ru) particle size (nm)				
							XRD[e]			H_2 uptake[f]	
	Before	After	Before	After	Before	After	Before	After	After[g]	Before	After
$Ni_{0.5}/Mg_{2.5}(Al)O$	173.6	56.8	120.7	40.2	13.1	4.4	6.8	18.4	n.d.	7.4	22.3
13.5 wt% Ni/γ-Al_2O_3	106.8	61.0	74.4	19.3	8.1	2.1	9.0	21.0	n.d.	12.0	46.4
0.01 wt% Pt-$Ni_{0.5}/Mg_{2.5}(Al)O$	142.8	–	160.2	–	14.6	–	6.3	–	–	6.6	–
0.05 wt% Pt-$Ni_{0.5}/Mg_{2.5}(Al)O$	144.0	–	169.9	–	15.5	–	6.4	–	–	6.3	–
0.1 wt% Pt-$Ni_{0.5}/Mg_{2.5}(Al)O$	141.2	56.9	225.3	44.3	20.6	4.0	5.5	16.5	10.0	4.7	24.0
0.5 wt% Pt-$Ni_{0.5}/Mg_{2.5}(Al)O$	152.0	–	224.1	–	20.5	–	5.1	–	–	4.7	–

[a] Steaming was carried out at 900 °C for 10 h in a $H_2/H_2O/N_2$ (20/100/25 ml min^{-1}).

[b] The catalysts were calcined at 800 °C for 5 h before catalytic tests.

[c] Determined by H_2 pulse method.

[d] Calculated from the H_2 uptake assuming the reduction degree of 80 % for hydrotalcite derived catalysts [15,39] and 100 % for impregnated catalysts.

[e] Calculated from the full width at half maximum of Ni (200) and Ru (101) reflections in the XRD using the Scherrer equation.

[f] Calculated using a equation: $d = 971/(\%D)/10$ where D is a dispersion [29].

[g] After steaming at 900 °C, followed by steam purged DSS SR operation between 200 and 700 °C.

Table 2. Turnover frequency of supported Ni catalysts before and after steaming.[a,b]

Before or After	Catalyst	CH_4 conversion (%)		H_2 uptake ($\mu mol\ g_{cat}^{-1}$)	TOF-s[c] (s^{-1})		TOF-t[d] (s^{-1})	
		500 ºC	600 ºC		500 ºC	600 ºC	500 ºC	600 ºC
Before	$Ni_{0.5}/Mg_{2.5}(Al)O$[e]	14.6	43.5	163.2	2.95	8.81	0.35	1.06
	0.10 wt% Ru-$Ni_{0.5}/Mg_{2.5}(Al)O$[e]	12.8	37.7	213.4	1.99	5.84	0.31	0.93
	0.10 wt% Pt-$Ni_{0.5}/Mg_{2.5}(Al)O$[e]	13.7	38.0	205.0	2.20	6.12	0.33	0.92
	13.5 wt% Ni/γ-Al_2O_3[f]	9.35	29.3	71.1	4.35	13.6	0.27	0.84
After	$Ni_{0.5}/Mg_{2.5}(Al)O$[e]	5.42	25.9	26.6	6.73	32.1	0.13	0.63
	0.10 wt% Ru-$Ni_{0.5}/Mg_{2.5}(Al)O$[e]	10.3	37.1	55.3	6.14	22.2	0.25	0.90
	0.10 wt% Pt-$Ni_{0.5}/Mg_{2.5}(Al)O$[e]	7.43	30.5	52.3	4.70	19.3	0.18	0.74
	13.5 wt% Ni/γ-Al_2O_3[f]	3.75	11.9	24.0	5.16	16.3	0.09	0.29

[a] Steaming was carried out at 900 ºC for 10 h in a $H_2/H_2O/N_2$ (20/100/25 ml min^{-1}). The catalysts were used as powders of 0.075-0.180 mm in diameter.

[b] SR of methane was carried out between 500-600 ºC in a $CH_4/H_2O/N_2$ (88.8/177.6/44.4 ml min^{-1}) at the GHSV of 1.6×10^6 ml $g_{cat}^{-1}\ h^{-1}$[e] or 3.6×10^5 ml $g_{cat}^{-1}\ h^{-1}$[f] after prereduction at 900 ºC for 0.5 h.

[c] TOF value was calculated based on surface Ni amount.

[d] TOF value was calculated based on total Ni amount.

Table 3. Curve fitting results of Ni *K*-edge EXAFS of 0.5wt%Pt-$Ni_{0.5}/Mg_{2.5}$(Al)O after reduction, steaming and DSS SR of CH_4[a]

Sample	Shells	C.N.	R / Å	σ / Å	ΔE_0 / eV	R_f / %
reduced [b]	Ni-Ni	7.9±1.3	2.49±0.01	0.072±0.02	-0.2±2.3	7.3
reduced-steamed [b]	Ni-Ni	7.2±1.3	2.48±0.01	0.059±0.02	-9.9±2.4	7.2
reduced-DSS [c]	Ni-Ni	6.8±2.4	2.46±0.02	0.099±0.02	5.3±5.2	10.3
	Ni-O	2.3±3.5	2.06±0.12	0.091±0.04	-10.8±5.9	
reduced-steamed-DSS [b]	Ni-Ni	8.5±1.5	2.48±0.01	0.068±0.02	-2.7±2.3	4.5
NiO[d]	Ni-O	6	2.02			
Ni foil[d]	Ni-Ni	12	2.49			

[a] C.N., coordination number; R, bond length / Å; ΔE_0, difference in the origin of photoelectron energy between the reference and the sample.; σ, Debye-Waller factor / Å; R_f, residual factor.
[b] $*R$ = 1.72 - 2.65 Å, $*k$ = 4 - 15.5 $Å^{-1}$.
[c] $*R$ = 1.09 - 2.65 Å, $*k$ = 4 - 15.5 $Å^{-1}$.
[d] Data from X-ray crystallography.

Table 4. Curve fitting results of Pt L_3-edge EXAFS of 0.5wt%Pt-$Ni_{0.5}/Mg_{2.5}$(Al)O after reduction, steaming and DSS SR of CH_4[a]

Sample	Shells	C.N.	R / Å	σ / Å	ΔE_0 / eV	R_f / %
reduced[b]	Pt-Ni	6.8±1.1	2.53±0.01	0.074±0.01	9.4±2.2	3.4
reduced-steamed[b]	Pt-Ni	6.7±1.1	2.52±0.01	0.090±0.01	1.9±2.3	19.5
reduced-DSS[b]	Pt-Ni	6.8±1.1	2.53±0.01	0.073±0.01	9.8±2.2	8.5
reduced-steamed-DSS[b]	Pt-Ni	7.7±1.2	2.54±0.01	0.081±0.01	9.8±2.2	5.4
PtO_2[c]	Pt-O	6	1.99			
Pt foil[c]	Pt-Pt	12	2.77			

[a] C.N., coordination number; R, bond length / Å; ΔE_0, difference in the origin of photoelectron energy between the reference and the sample.; σ, Debye-Waller factor / Å; R_f, residual factor.
[b] $*R$ = 1.78 - 2.57 Å, $*k$ = 4 - 16.0 $Å^{-1}$.
[c] Data from X-ray crystallography.

Table.5. Curve fitting results of Ru *K*-edge EXAFS of the 0.5wt%Ru-$Ni_{0.5}/Mg_{2.5}$(Al)O catalyst after reduction and DSS ATSR of CH_4[a]

Sample	Shells	C.N.	R / Å	σ / Å	ΔE_0 / eV	R_f / %
0.5 wt% Ru-$Ni_{0.5}/Mg_{2.5}$(Al)O[b]	Ru-Ni	3.7±0.8	2.49±0.01	0.079±0.02	-12.9±2.9	3.0
0.5 wt% Ru-$Ni_{0.5}/Mg_{2.5}$(Al)O[c]	Ru-O	3.8±0.6	2.07±0.01	0.064±0.02	9.2±2.0	0.8
RuO_2	Ru-O	6				
Ru metal	Ru-Ru	12	2.66			

[a] C.N., coordination number; R, bond length / Å; ΔE_0, difference in the origin of photoelectron energy between the reference and the sample.; σ, Debye-Waller factor / Å; R_f, residual factor.

[b] After reduction.

[c] After DSS ATSR.

Figure 1. K. Takehira et al

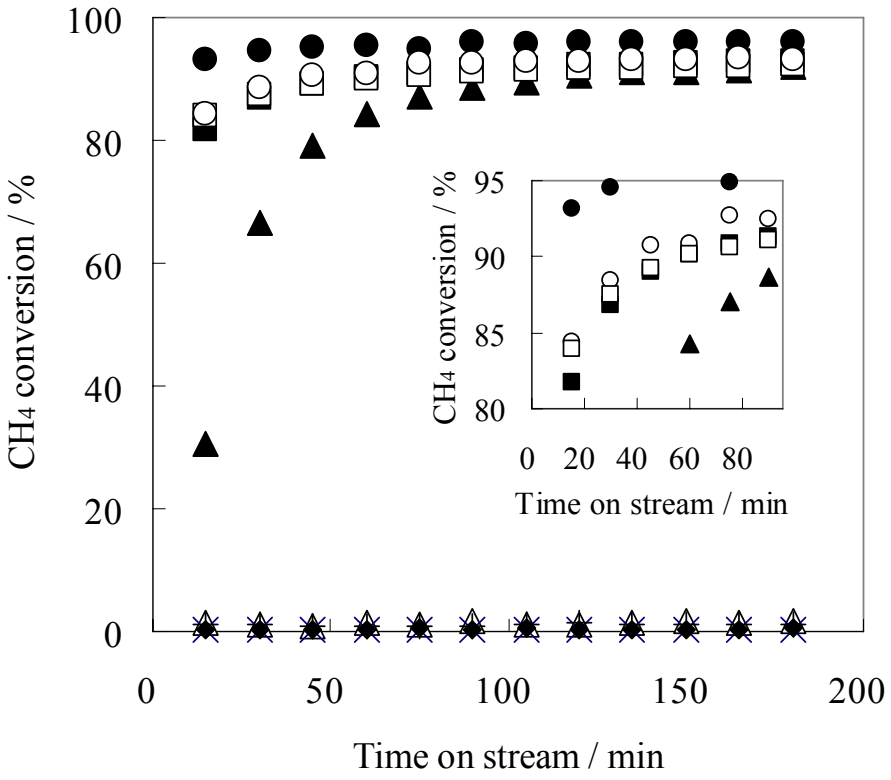

Figure 2. K. Takehira et al.

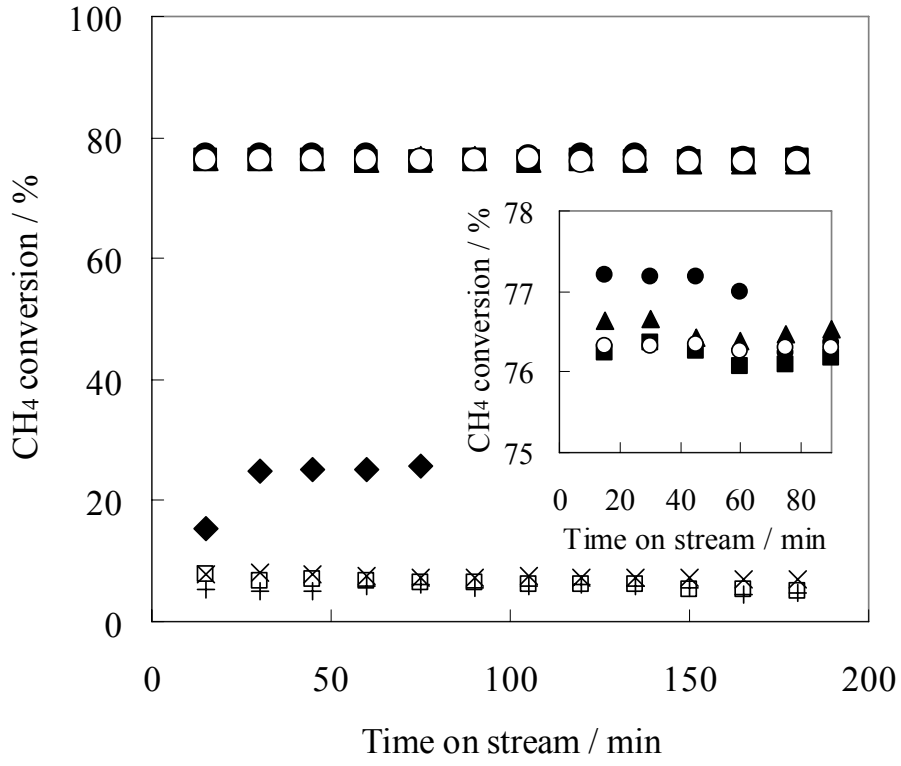

Figure 3. K. Takehira et al.

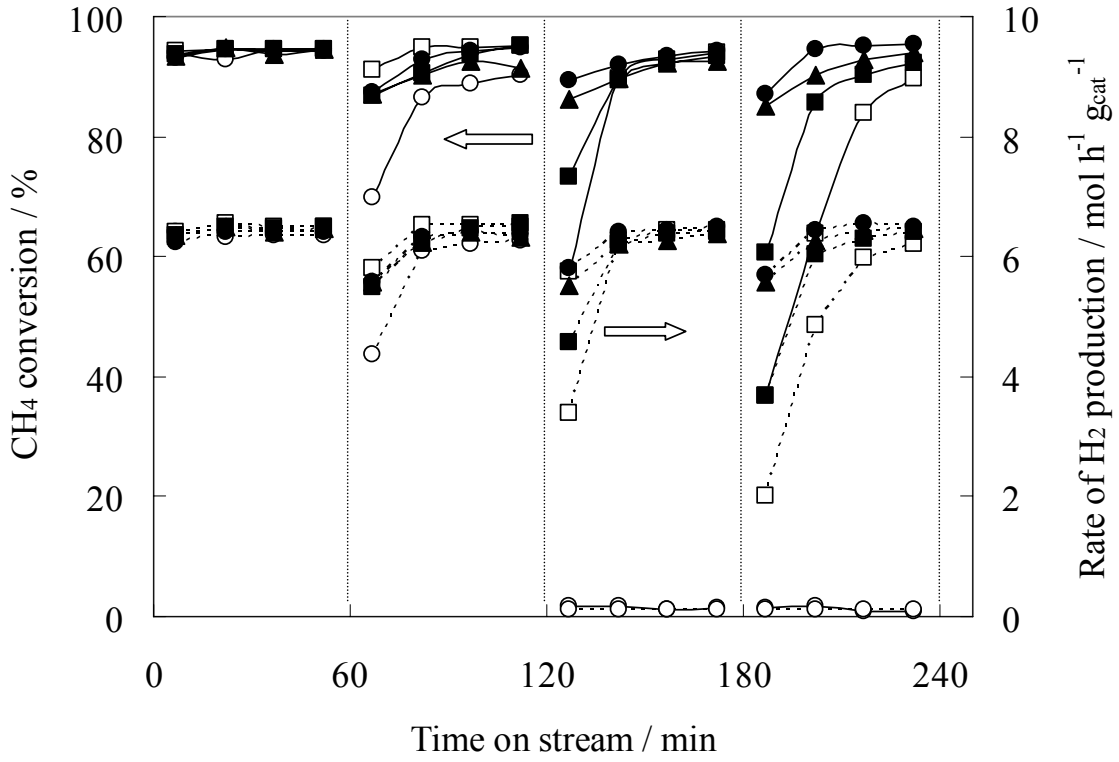

Figure 4. K. Takehira et al.

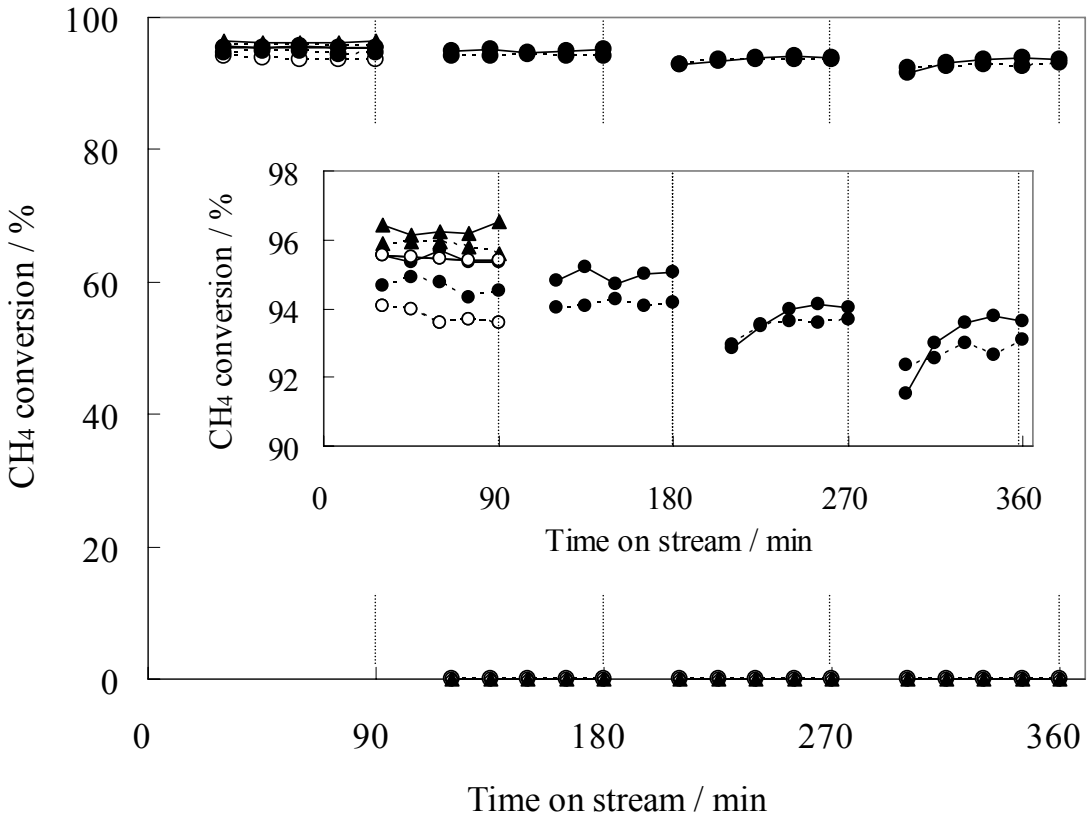

Figure 5. K. Takehira et al.

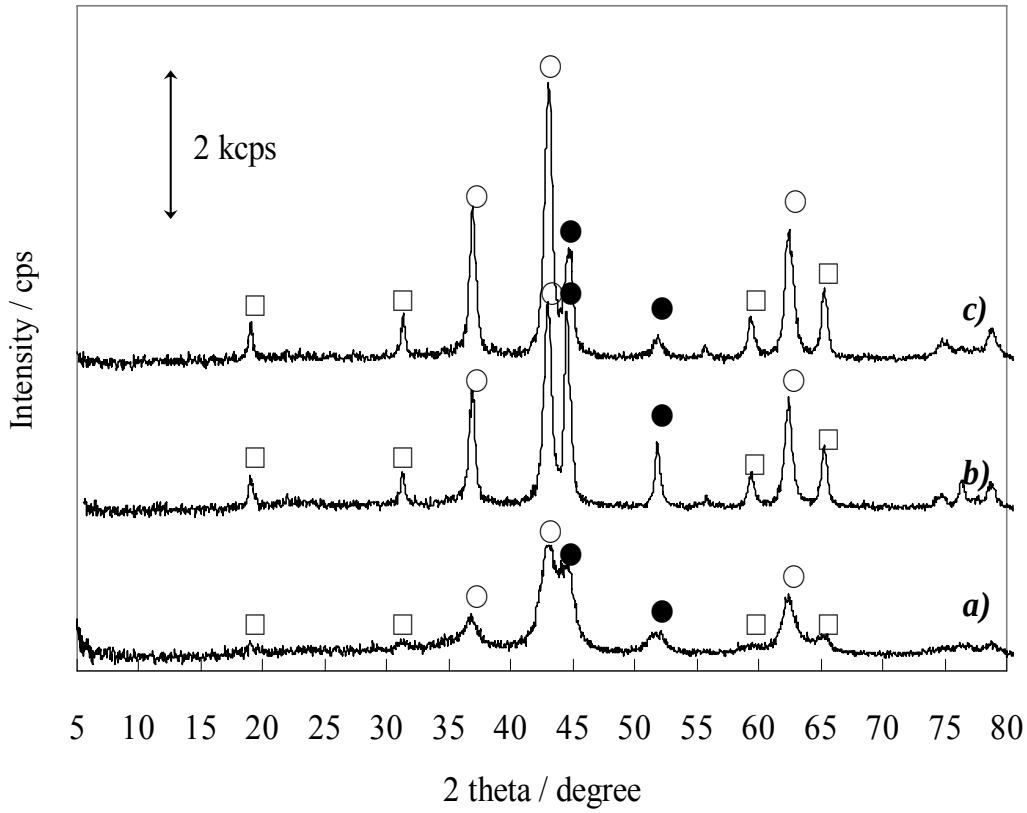

Figure 6. K. Takehira et al.

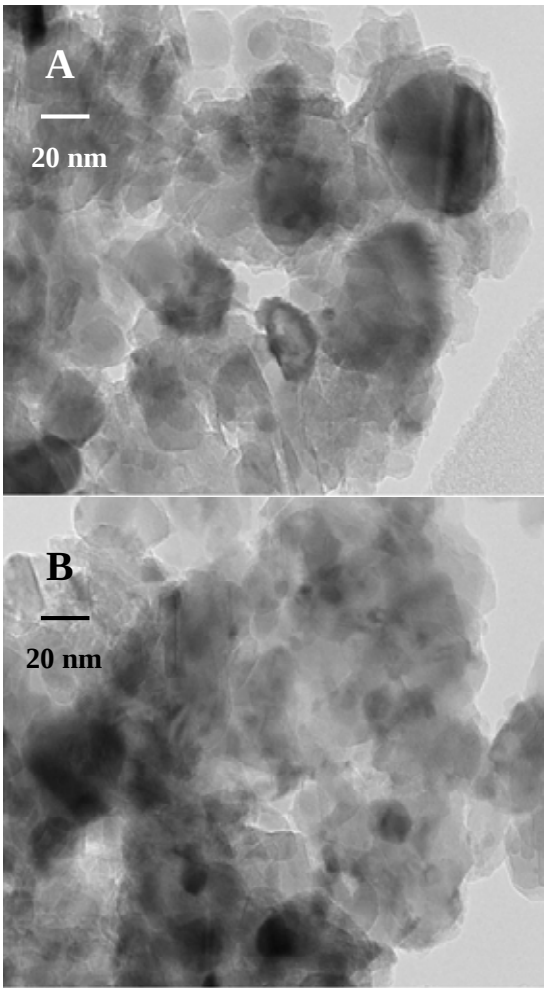

Figure 7. K. Takehira et al.

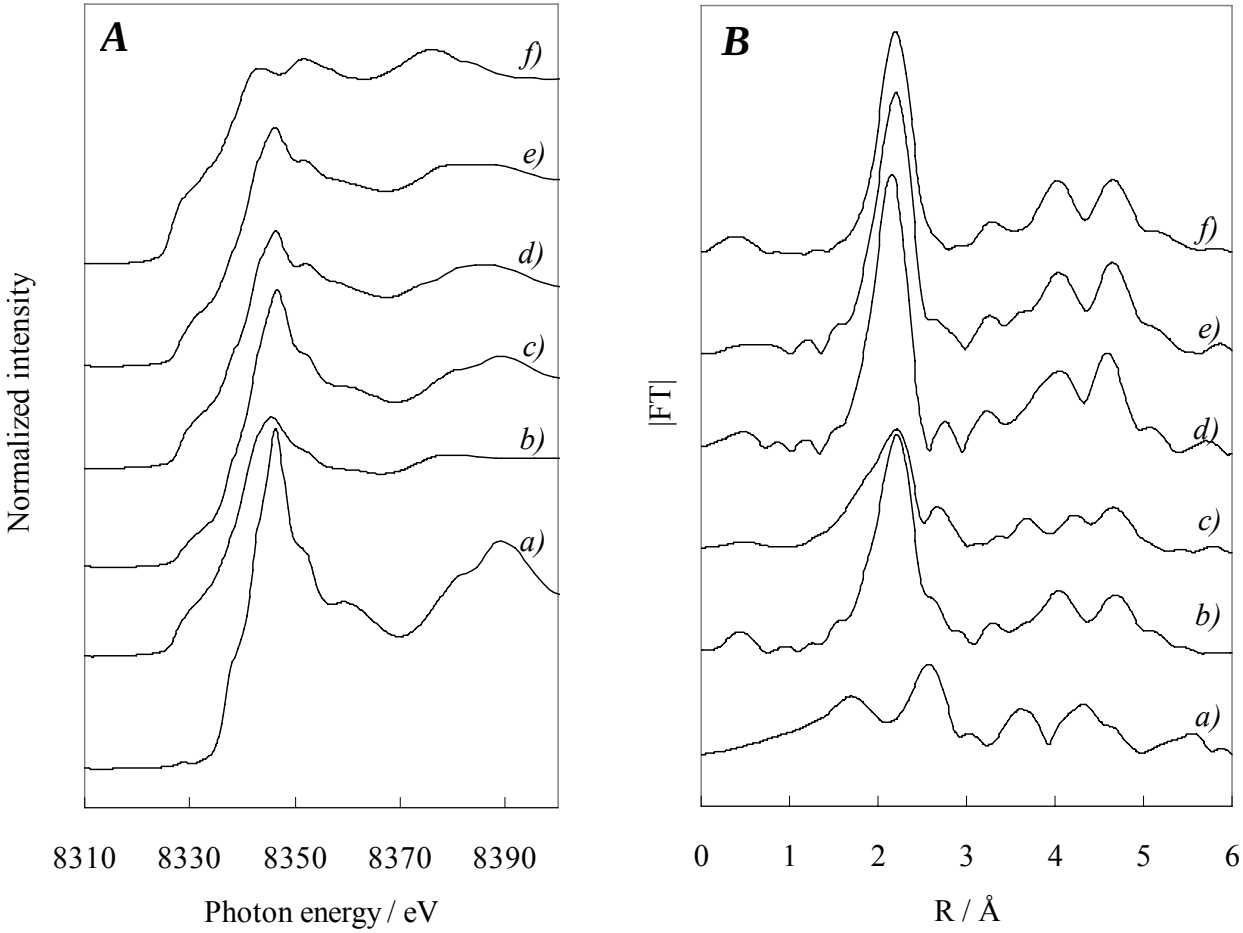

Figure 8. K. Takehira et al.

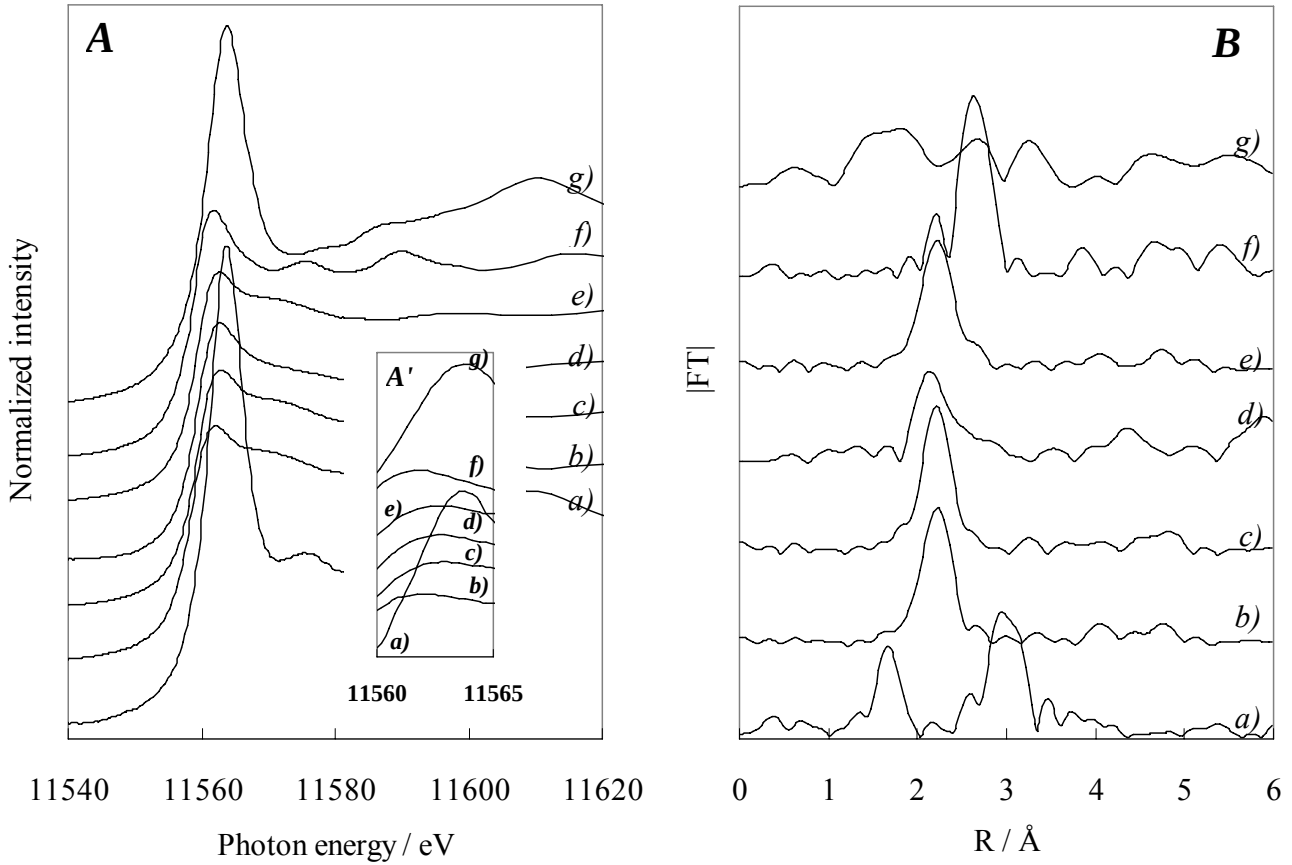

Figure 9. K. Takehira et al.

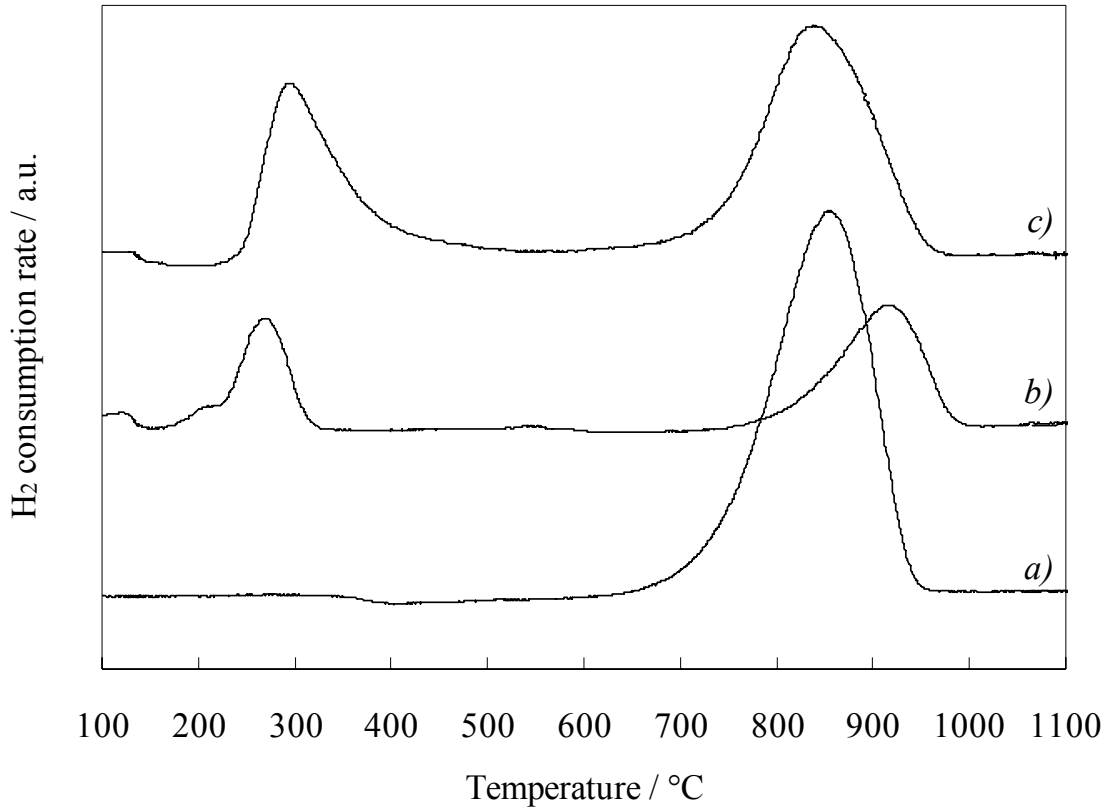

Figure 10. K. Takehira et al.

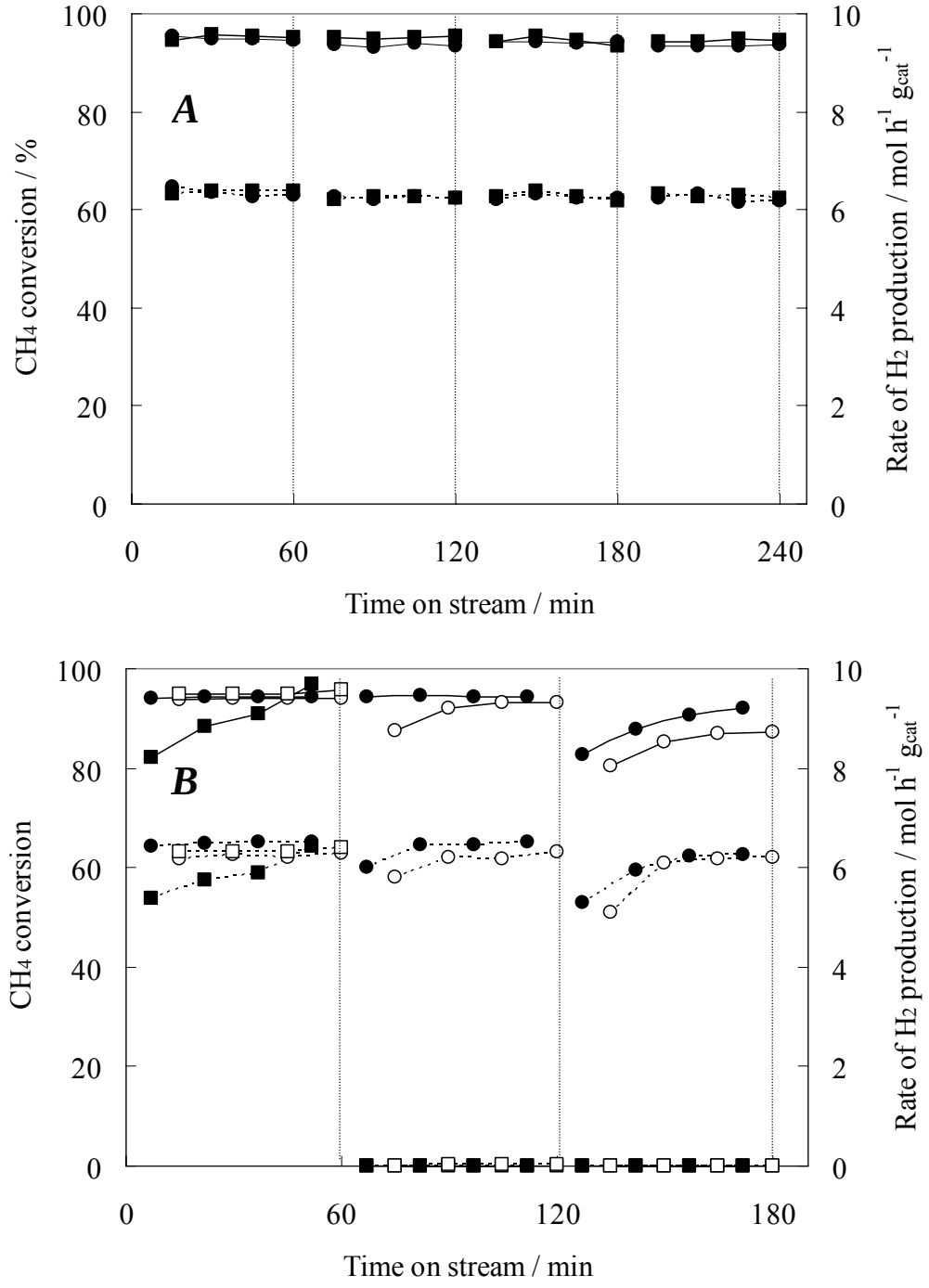

Figure 11. K. Takehira et al.

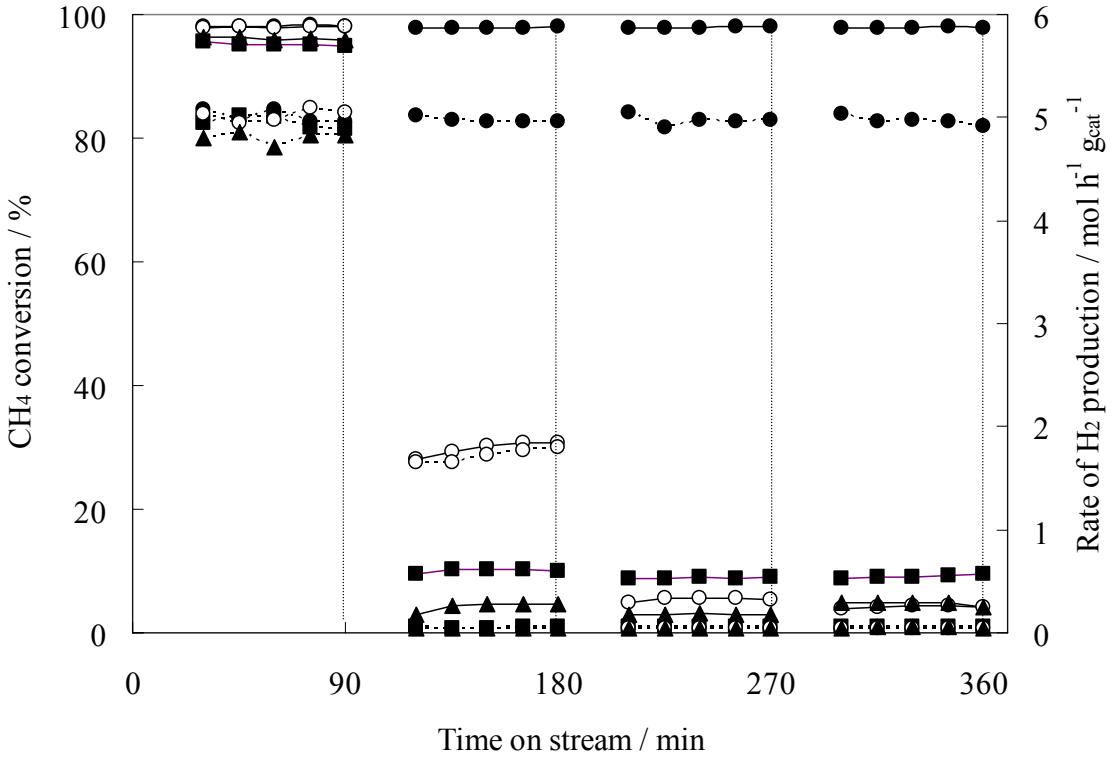

Figure 12. K. Takehira et al.

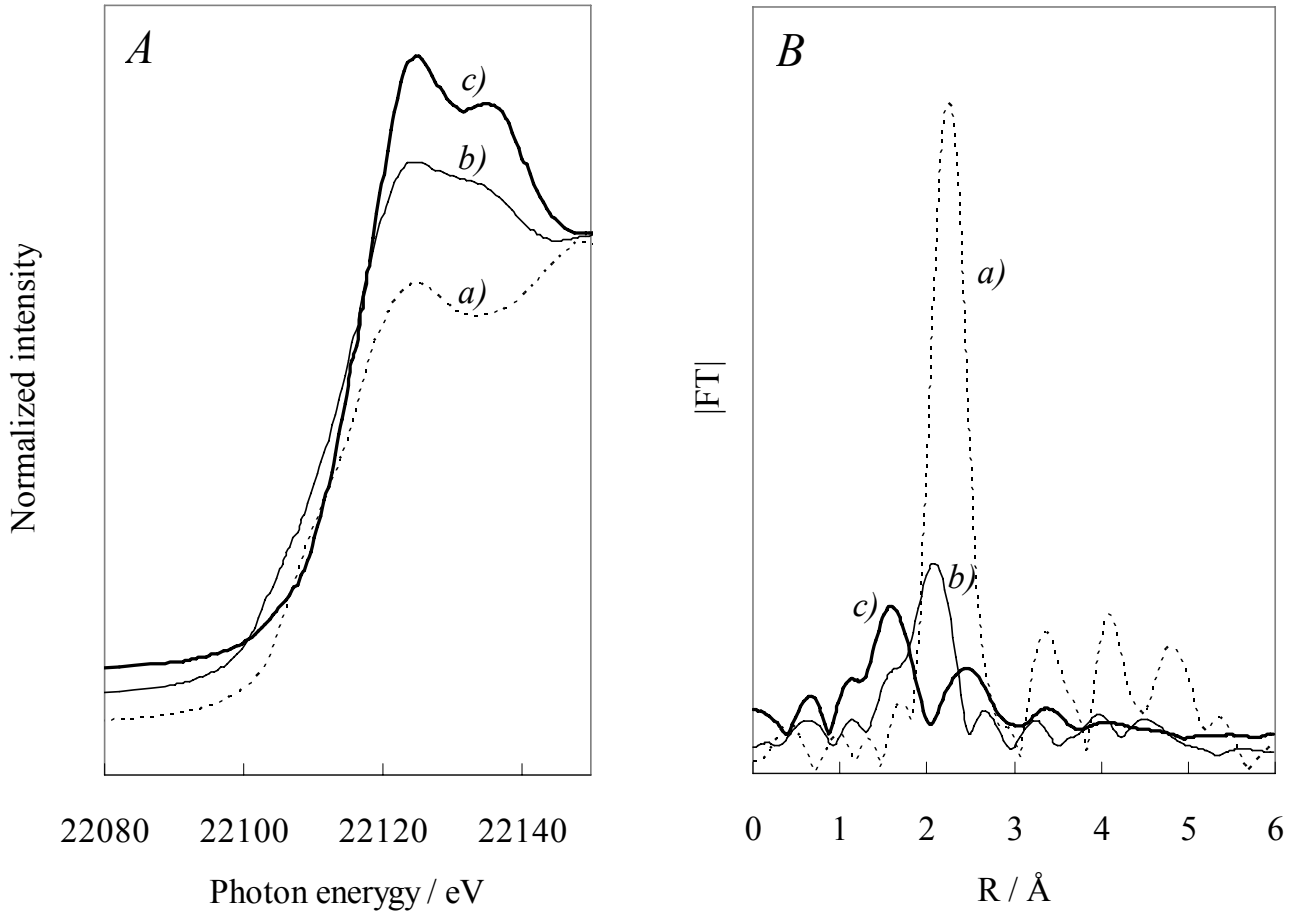

Scheme 1. K. Takehira et al.